UNIVERSITÄT LEIPZIG
Fakultät für Lebenswissenschaften
Institut für Biologie

What is the surface of a tree?

Understanding branch surface to volume allometry using terrestrial laser scanning.

Abschlussarbeit zur Erlangung des akademischen Grades

Bachelor of Science (B.Sc.)

vorgelegt von

Tobias Meißner

Geb. am 20.06.1989 in Leipzig

Gutachter: Prof. *Christian Wirth*

Gutachterin: Prof. *Alexandra Weigelt*

Erklärung

Ich versichere hiermit, dass ich die vorliegende Arbeit selbständig verfasst und keine anderen als die im Literaturverzeichnis angegebenen Quellen benutzt habe.

Alle Stellen, die wörtlich oder sinngemäß aus veröffentlichten oder noch nicht veröffentlichten Quellen entnommen sind, sind als solche kenntlich gemacht.

Die Zeichnungen oder Abbildungen in dieser Arbeit sind von mir selbst erstellt worden oder mit einem entsprechenden Quellennachweis versehen.

Diese Arbeit ist in gleicher oder ähnlicher Form noch bei keiner anderen Prüfungsbehörde eingereicht worden.

Leipzig, den *30.09.2019*

Summary

The surface area exposed by branches of tree canopies has significant implications for many eco-physiological processes such as stem respiration and the interception of light and rain. In addition, the surface provides the habitat area for colonization of numerous taxa such as lichens, algae and bark-dwelling arthropods. Despite its high ecological relevance, the surface characteristics of tree canopies remain so far understudied because of the high effort needed to quantify this architectural trait accurately and non-destructively.

We aim to investigate how variations in tree surface allometries between species can be explained. We hypothesize that those differences are driven by species-specific architectural traits. More precisely, we expect that small terminal branch diameter indicate a higher bifurcation frequency, resulting in a higher tree surface area.

We thus propose a semi-automatic method based on terrestrial LiDAR scans in order to extract architectural information of six European tree species in an alluvial forest at the Leipzig Canopy Crane research site. First, we developed a method that detects and segments individual trees from the LiDAR point-cloud semi-automatically. Subsequently, we computed three-dimensional quantitative structure models (QSM) of the LiDAR point cloud. As a final step, we calculated the volume and surface area using the QSMs.

This enabled us, for the first time, to develop allometric equations needed to quantify surface area distribution in the complex three-dimensional ecosystem compartment of tree crowns for biodiversity and eco-physiological research. We show that species with a small terminal branch diameter like *Carpinus betulus* exhibit significantly larger surface areas compared to species with thicker terminal branches like *Fraxinus excelsior*. The differences in surface area emerging between species can be explained by the species-specific terminal branch frequency defined by the terminal branch diameter. Thus, we use the terminal branch diameter as a proxy for branching frequencies. Most importantly, we present an innovative and generalized allometric equation to quantify the surface area of tree species not included in this thesis.

We can conclude, that tree species differ in their tree surface area, but not in their wood volume, and that those differences are related to tree architectural parameters. Therefore, we accept both of our hypotheses.

Danksagungen

Ich möchte mich bei all denjenigen Menschen bedanken welche mich bei der Anfertigung meiner Bachelorarbeit unterstützt und motiviert haben.

An erster Stelle seien hier Prof. Christian Wirth und Prof. Alexandra Weigelt genannt, welche mir nicht nur die Möglichkeit gaben diese umfangreiche Aufgabe zu aufzunehmen, sondern mir dies auch in sehr großer Eigenständigkeit zu getraut haben. Ich hatte jederzeit die Gewissheit, dass ihre konstruktiven Anregungen und Hinweise einem fundierten Fachwissen entspringen und mich im Schaffungsprozess positiv beeinflussen.

An zweiter Stelle will ich Ronny Richter nennen, welcher mir bei Tag und Nacht hilfreich zur Seite stand um mit mir feinste Details der Statistik und der Datenauswertung zu diskutieren. Nie werde ich die frühlingshafte Kranfahrt in den Kronendächern des Forschungsgebietes des Leipziger Auwaldkranes vergessen, welche ich bis dato nur in digitalen Repräsentationen der mir zur Verfügung gestellten Scandaten kannte.

All dies wäre jedoch nicht möglich gewesen ohne die Unterstützung meiner langjährigen Arbeitsgruppe der Zahnerhaltung und Parodontologie unter der Direktion von Prof. Rainer Haak und meinem sehr geschätzten Laborleiter Dr. Hartmut Schneider. Die uneingeschränkte Bereitstellung von mehreren Workstations und der Laborräume war die einzige Möglichkeit die enormen Datenmengen zu prozessieren. Ebenso möchte ich meinen Dank meiner ebenso langjährigen Kollegin Claudia Rüger aussprechen. Welche mir immer mit hilfreich offenen Ohren für meine Probleme und Sorgen mit Rat und Tat beiseite stand.

Nun folgend, jedoch nicht minder wichtig, will ich mich bei Maximilian Bemmann bedanken. Welcher Dank seiner fundierten Matlab und R Kenntnisse mir nicht nur einmal Stunden der Suche nach der besten Lösung ersparte.

Ebenso essentiell für mein Weiterkommen waren Claudia Guimarães-Steinicke sowie Daniel Seifarth. Bei beiden möchte ich mich für die geleistete Unterstützung bedanken. Ohne Claudia wäre die iDiV Konferenz 2019 für mich nicht so erfolgreich verlaufen und ohne Daniel hätte ich mit hoher Wahrscheinlichkeit weniger Fokus auf das Wesentliche gelegt und noch weniger eigene Fehler gefunden.

Großem dank bin ich auch Prof. Rudolf Rübsamen schuldig, welcher mich in jungen Jahren an die wissenschaftliche Arbeit heranführte und mir während meines Werdeganges steht's wohlgesonnen in Freundschaft Ratschläge und offene Ohren bot.

Zum Schluss möchte ich mich bei meinen Eltern Vera und Thomas Meißner sowie meinem großen Bruder Daniel Meißner bedanken. Meine Eltern standen im gesamten Studium unterstützend hinter mir und mein Bruder sorgte zusammen mit Alexandra und meinen Neffen Mateo immer für genügend körperlicher und geistiger Zerstreuung.

Tobias Meißner, Leipzig den 30.01.2019

Table of Contents

1. Introduction

1.1. Tree Surface and Tree Allometry

The surface of a tree or as referred to in this bachelor thesis the tree surface area is the outer shell of the bark, including the stem, branches and twigs without leaves. During normal growth trees bifurcate at a species-specific rate. Scientific interest in those species-specific patterns dates back to at least Leonardo da Vinci, who first observed that cross-sectional area of branches is preserved along branching orders within a tree [1,2]. The “pipe-model” described for the first time in 1964 by Shizonaki et al. [3–5] states that the overall cross-sectional diameter of a tree remains the same after each bifurcation. The design of branching architectures is hypothesized to reflect trade-offs to access and fill three-dimensional space in order to transport resources with maximum efficiency and minimal cost [6].

The tree surface area emerges as a consequence of species-specific traits with, the above mentioned branching architecture and the bark structure being the most important ones [1]. The exposed tree surface area of branches of tree canopies has significant implication for many eco-physiological processes [7] such as stem respiration [8,9] and the interception of light and rain, but also provides the habitat area for colonization of numerous taxa such as mosses [10,11], lichens [11–14], algae [15,16] and bark dwelling arthropods [17,18]. A commonly used method for estimating the total woody tissue respiration measures the emanating carbon dioxide at a given area on the bark surface. These measurements are then scaled up with allometric assumptions for the whole tree. Therefore, an exact prediction of the tree surface area is important [19,20]. Most studies focus on the bark and how the structure influences the associated organisms [21,22]. In addition, tree surface has an impact how stem flow is modulated [23]. Little is known how species-specific characteristics like branching patterns and twig diameter influence tree surface. Few studies have examined the surface area allometries of trees and except for the study of Pokorný and Tomášková [24] most of these studies focused on total leaf area [25] or the leaf area index [26–28].

Allometry is the study of the relationship between dimensions of different traits of an organism. One of the first relationships between the primary cross-sectional area of a stem and surface area of the leaf borne by it was recognized by Corner et al. [29–31]. In contrast, many studies revealed the relationship between diameter at breast height (DBH) and total

tree height and volume and therefore allometric equations for many species are available [32,33]. Those are important predictors for biomass and carbon sinks. Although, the tree surface has a high ecological relevance, surface characteristics of tree canopies remains so far understudied. Because large scale or even forest sized tree canopy studies were linked with a very high labor costs particularly for anything other than small trees [34]. Most canopies are not easily accessible. Therefore, the main focus on tree surface was restricted to the lower part of trees. As well the measurement of such characteristic's as volume and surface area are extremely laborious determinable and in most cases destructive.

1.2. Remote Sensing and Terrestrial Laser Scanning

In the last decades the use of three-dimensional analysis in the fast developing field of Remote Sensing gained a great deal of attention[35]. Remote sensing is a field which uses technology to acquire information about objects from a great distance. Commonly by means of satellite- or aircraft-based sensor technologies [36,37]. Terrestrial LiDAR scanning (TLS), a method which uses the reflectivity of objects is commonly known as "light detection and ranging" (LiDAR). This method uses a red or near-infrared laser beam to scan the surrounding. Since the angles of the x- and y-axis are known, only the distance from the reflectance needs to be calculated using the time which the light needs to be detected by a sensor. The position of each reflection can be geo-referenced. A huge advantage of this method is high dimensional accuracy and the speed. In addition, the scanner can be coupled with a digital camera to record color information as well. The generated data, called point clouds [38] is then accessible and analyzable through a variety of free and commercial software.

Today, research in forestry or tree architecture is generally on the brink of a technology-driven revolution since new affordable and field-robust terrestrial laser scanning technologies are released [1,39]. Those devices are now available for foresters and ecologists and they are used to obtain forest and tree characteristics [40,41]. Mainly used for applications in architecture and geoscience for mapping of surfaces and areas, the data processing routines had to be adapted to the new field for forest sciences. One of the advances in the data acquisition and analysis is the linking of many scan-positions across wide areas using registration targets [42]. In combination with the use of full or semiautomatic [43–45] approaches for tree segmentation terrestrial laser scanning is

becoming an accurate, non-invasive objective and repeatable option to address multiple scientific questions related to tree architecture [46].

1.3. Quantitative Structure Models

Eventually, terrestrial laser scans allow us to quantitatively describe the structure of a large number of trees. Most of the studies focus of how biomass or leave foliage is distributed using approaches like random branch sampling [47,48]. Those methods are manageable by humans with a decent amount of time and effort. Having said this, it is important to mention that by this not the whole tree is quantified and uncertainties remain high. With an increase in effort and time one could increase the accuracy of the quantifiable variables. With available technologies which are used in remote sensing the workload for humans is greatly reduced and even large forest can be monitored. Using LiDAR from attached on airplanes it is now possible to calculate the mean diameter at breast height (DBH) and biomass without even setting a foot in a forest [37]. To calculate those traits one can make use of a quantitative structure model (QSM) [43–45]. Basically a QSM is a collection of hierarchical ordered geometric shapes fitted into terrestrial laser scanning point clouds. With structure models as these, when extended to a large quantity of individuals we are now able to develop a robust understanding on the relationship between tree architecture, tree surface area and other traits.

1.4. Hypothesis

Tree specific architectural traits like bifurcation patters or terminal branch size are suspected to influence the tree surface area. At a given point in growth of a tree, branches bifurcate in order to maximize their efficiency of resource use. At every bifurcation point, the branch is divided into progressively smaller branches and the resulting surface area increases with the total number of terminal branches inversely proportional to their diameter. Therefore, we can use the terminal branch diameter as a proxy for branching intensity. At a given volume of the parent branch or even a whole tree we can use this relationship as a predictor for surface area of the tree .Arising questions of the concept of the pipe model, the branching architecture in combination with Corner’s rule are formulated with the following hypothesis:

a) At a given size, tree species differ greatly in total tree surface area, but not in their wood volume.
b) These differences are related to tree architectural parameters such as terminal branch diameter and branching intensity.

1.5. Aim of the Thesis

This bachelor thesis is aiming to answer scientifically questions regarding tree species-specific traits in context with tree surface area and volume. More specifically, we aim to investigate how variations in tree surface allometries can be explained. We hypothesize that those differences are driven by species-specific architectural traits. More precisely, we expect that small terminal branch diameter indicate a higher bifurcation frequency, resulting in a higher tree surface area. To achieve this, we aim to develop a semi-automatic workflow to process large point clouds created with terrestrial laser scanners in order to segment six different European tree species into a sufficient amount and size distributed high quality individual tree point clouds. In addition, we aim to compute quantitative structure models to extract species-specific architectural traits like total tree surface area, tree volume, bifurcation patterns and terminal branch diameters. Allowing us to establish relationships between tree architecture and volume respectively tree surface area.

2. Materials and Methods

2.1. Study Area

The study was conducted at the Leipzig Canopy Crane (LLC) research site (51°20'16"N; 12°22'26"E, 102 m above zero) in the nature reserve of the *Burgaue* of the hard-wood floodplain forest of Leipzig. The species and structurally-rich woodland is situated at the margin of a former oak and elm rich floodplain forest. (*Querco-Ulmetum monoris* ISSLER)[49]. The site is in the transition zone from the oceanic and continental climate zone and has a temperate climate. The precipitation ranges from 34 mm to 77 mm per month with an annual total of 592 mm (multiyear precipitations means from 1981 – 2010) [50]. Mean temperature is ranging from 2.9°C in winter and 23.7°C in summer. The area is close to two rivers and is part of a bigger alluvial forest.

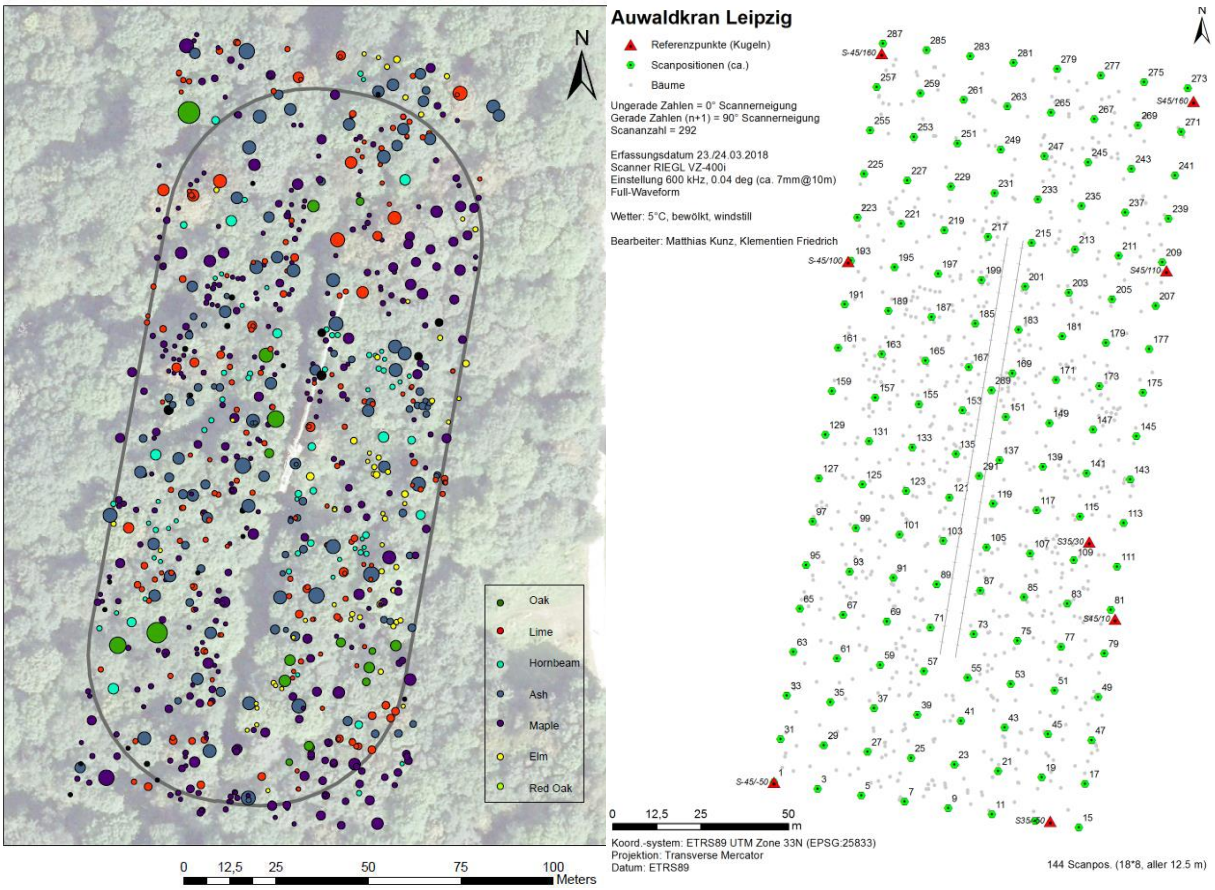

Fig. 1: Representation of the *Leipzig Canopy Crane (LLC)* study area. Left hand graphic is visualizing the different tree individuals color coded by species. Right hand graphic is showing in green the scanning positions and in red the georeferenced markers. Grey dots represent stem positions. Two scanning positions and the crane track are not included in this graphic [51].

The plot is about 1.6 ha in size and includes approximately 800 individual trees of 15 species [52] (> 5 cm diameter at breast height – DBH) (**Fig. 1**).

2.2. Data Collection using Terrestrial Laser Scanning

To obtain structural information about different tree characteristics using a nondestructive method the study area was scanned using terrestrial laser scanning (TLS). Data collection of point clouds took place on March 23th and 24th in 2018. Weather conditions were stable and the air temperature was about 5°C with a fairly cloudy sky. Furthermore, the impact of wind was negligible and therefore a double or shadow capturing of branches can be excluded.

To capture the entire plot (**Fig. 1**) the working group of biodiversity and nature conservation of Prof. Goddert von Oheimb from the technical university Dresden scanned in total 144 positions on a grid of 12.5 m. A Riegl VZ-400i (Laser class 1, 1550 nm) was used (**Fig. 2**). In addition, each position was scanned twice on a height of approximately 1.3 m. The angular resolution was 0.04° which corresponds to a spatial resolution of roughly 7 mm within a 10 m radius. To ensure a good cover of each scan a vertical field of view of 100° and a horizontal field of view of 360° was used. Additionally, settings were set to active full-waveform and a scan frequency of about 600 kHz. Thus, four to eight targets per laser pulse could be recorded, resulting in a very good cover of all tree-segments. Nevertheless, small occlusions of higher elements in the canopies couldn't be excluded [53].

Fig. 2: Riegl VZ-400i in the field at the Leipzig Canopy Crane (LLC) Plot. Pictures provided by the project report [51].

Secondly, seven reference markers and the software RiSCAN PRO (v. 2.6.2) [54] were used for registration and geocoding (ETRS89_UTM33) of all scans.[51] Accordingly, the accuracy of the relative registration is about 5 mm and the absolute accuracy is about 50 cm. In addition, the quality of the point clouds was examined and noise and outliers were removed [51]. Ultimately the total dataset size of the 292 scans amounts to 125 GB.

2.3. Point Cloud Preparation and Sub Sectioning

The quantitative structure model computing process accepts individual tree point clouds as input data. Furthermore, before we could start segmenting our target trees into individual point clouds we needed to prepare the point clouds of every scan position. It is important to mention that a target tree is a tree with a diameter at breast height larger than 5 cm and one of the following species: *Acer platanoides* L.*, Acer pseudoplatanus* L.*, Carpinus betulus* L.*, Fraxinus excelsior* L.*, Tilia cordata* Mill. and *Quercus robur* L.. As a reference data from a forest inventory (2015) including tachymetric measured geo-positions, tree dimensions and species names were used. Therefore, every tree had a unique identification number affiliated with the geocoded position of the stem. Using this information we developed a windows command line batch script (**appendix: i**) to sub section, or more precisely crop, the point clouds of all scan positions. We use a different font with capital letters for discrimination of Cloudcompare [55] and Computree [56] plugin names from normal text. In essence, we used the plugin `CROP2D` from software the CloudCompare to crop a hexagonal shaped plot defined by a 30 m diameter inscribed circle (**Fig. 3a - d**).

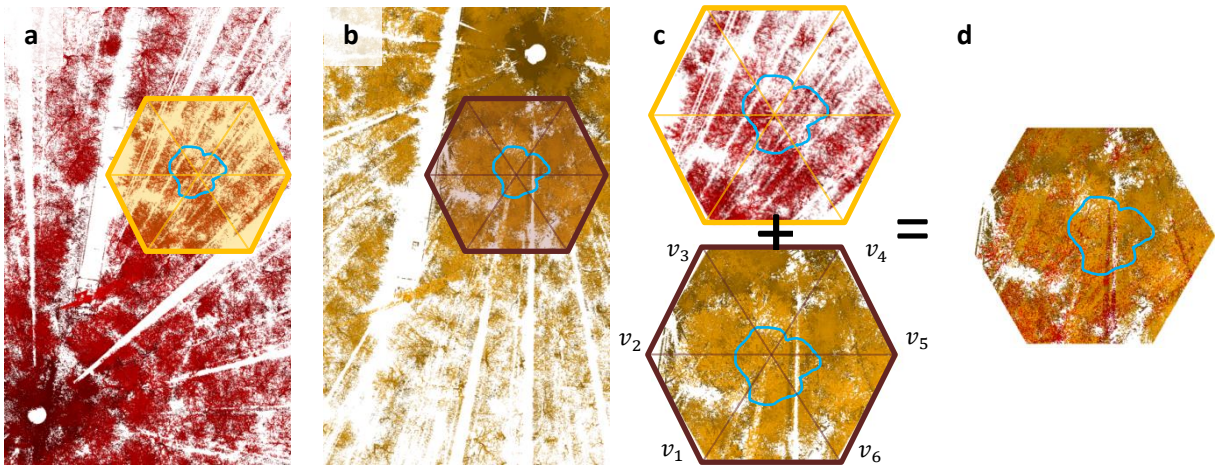

Fig. 3: Exemplary workflow of sub-sectioning and merging of point clouds. For demonstrational purposes only two scanning positions with a very large distance are presented. **a**) One out of 146 scans (red) with a hexagon shaped plot with the target tree in the center, canopy is highlighted in blue. **b**) Second scan position (amber) with highlighted sub-section and canopy. **c**) Created subsections with the CloudCompare plugin `CROP2D` and target tree canopy in blue. **d**) Final merged point cloud.

The script accepts a list (l) of six vertices (**Fig. 3c**) and an ASCII formatted point cloud (p). We calculated the vertices as shown in **Tab. 1**. If the radius of the inscribed circle is r then the circumference is (**1**)

$$c = 2\pi r \quad (1)$$

while a side of the hexagon is (**2**).

$$s = {}^{2}/_{\sqrt{3}}\, r \quad (2)$$

Tab. 1: Formulas for the calculation of vertices ($\boldsymbol{v_n}$), $\boldsymbol{N}$ = northing, $\boldsymbol{E}$ = easting, $\boldsymbol{s}$ = side of hexagon, $\boldsymbol{x_1} \dots \boldsymbol{x_n}$ = x coordinates, $\boldsymbol{y_1} \dots \boldsymbol{y_n}$= y coordinates.

$\boldsymbol{v_1}$		$\boldsymbol{v_2}$		$\boldsymbol{v_3}$		$\boldsymbol{v_4}$		$\boldsymbol{v_5}$		$\boldsymbol{v_6}$	
$\boldsymbol{x_1}$	y_1	x_2	y_2	x_3	y_3	x_4	y_4	x_5	y_5	x_6	y_6
$\boldsymbol{E-\frac{s}{2}}$	$N-s$	$E-s$	N	$E-\frac{s}{2}$	$N+s$	$E+\frac{s}{2}$	$N+s$	$E+s$	N	$E+\frac{s}{2}$	$N-s$

By doing so we ensured that the stem of the target tree is in the center and even the largest tree canopy was inside the sub-section. Furthermore, we now needed to merge the sub-sectioned point clouds. This is an important step to make sure that we use the maximum number of points available for the target tree. Therefore, we developed a second batch script using the `MERGE_CLOUDS` plugin of CloudCompare see **appendix ii** and **Fig. 3d**. This leads us to another issue because point clouds smaller than 4 MB do not provide sufficient structural information and might include possible artifacts caused by wind. Consequently, exclusively point clouds larger than 4 MB were accepted as input. This procedure was repeated for all target tree individuals. In the end all point clouds were stored as a binary `xyb` file. By this we ensured a shorter processing time during the segmentation process.

2.4. Segmentation into Individual Tree Clouds

As stated in section 2.3 the QSM computing process only accepts individual tree point clouds as input. Given that, we developed a workflow using Computree which semi-automatically segments the hexagonal point clouds into individual target tree point clouds. Taken together, we were able to detect all sizes of trees with good to very good precision. Thus, manual interference could be minimized. A summary of the script can be found in **appendix iii**. Hereafter, a short description for better understanding of the script is presented. A visual representation of that process is shown in **Fig. 4**.

Firstly, we imported one merged hexagonal shaped `xyb` point cloud (**Fig. 4a**).

As a next step we needed to discriminate between vegetation and ground points. This was done by classifying ground points (`Classify Ground Points (TLS)`). In this step a Z_{min} raster is created where each pixel contains the Z value of the lowest point. Additionaly, this raster is filterd to discard aberrant points based on two optional criteria. The density of points and the coherence of the neighboring points. All points above those unfiltered points on a fixed, but user defined, thickness are classified as ground points (**Fig. 4b**).

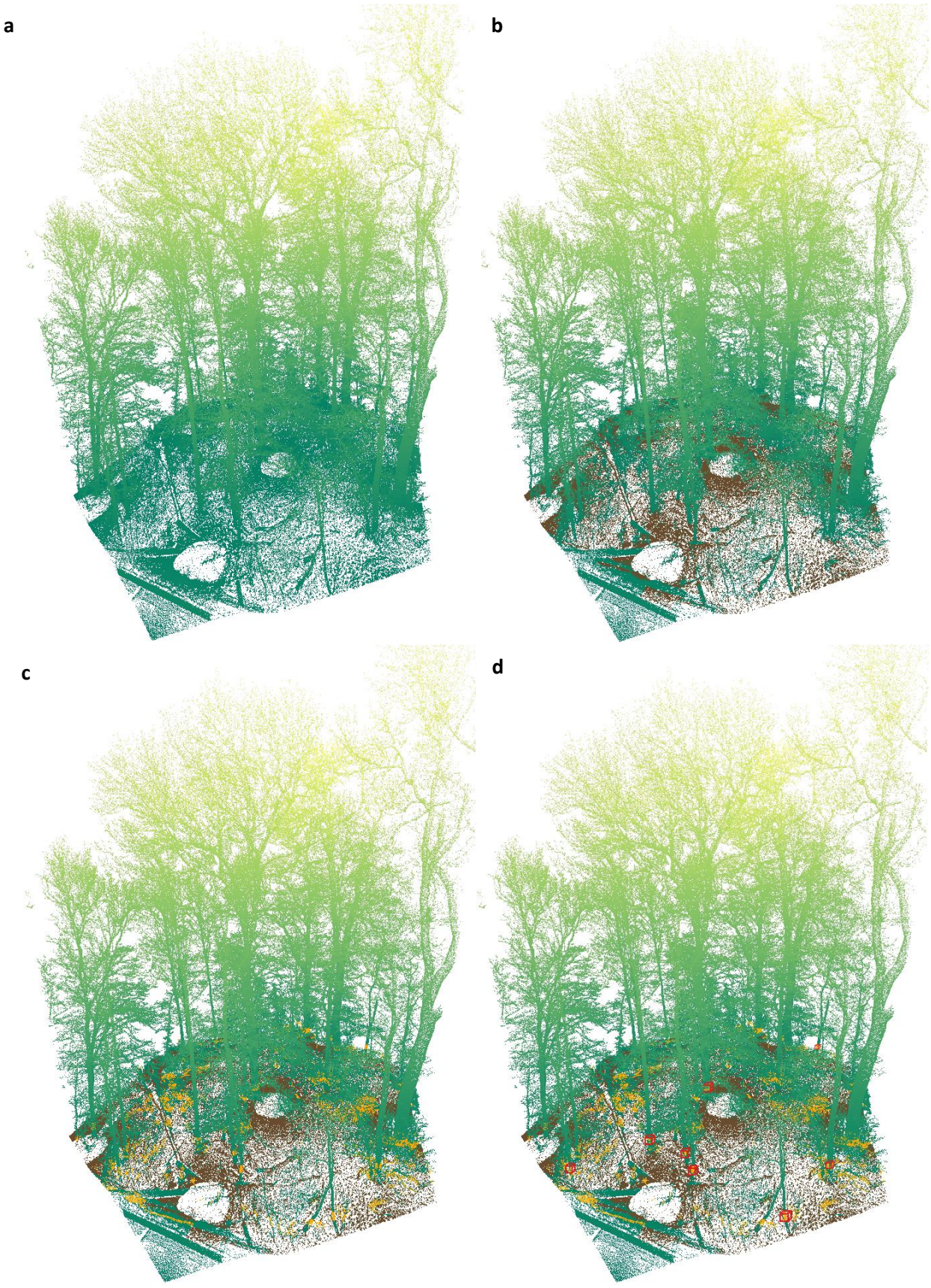

Fig. 4: Visual representation of a 30 m hexagon shaped subplot. For demonstrational purposes the presented point cloud contains ten times fewer points than the original. Circles on the ground containing no points are the scan positions. **a**) One exemplary 30 m hexagonal sub section. **b**) Classified Ground Points (brown) and vegetation point cloud (green to yellow).**c**) A 60 cm thick extracted slice of (orange) for stem detection. **d**) Detected stems represented with red cubes.

With those two separate point clouds we are able to compute a digital terrain model (`Create DTM` [57]). This is needed to compensate for height differences in the plot area. Important parameters for this step is the grid resolution and the interpolation algorythmus needed if ground points are missing.

We can now use this DTM for the detection of stem positions in our plot. This is done by smoothly extracting a slice parallel to the DTM using the plugin developed by Hackenberg `Smooth Extraction Of A Point Slice Parllel To The DTM` [58,59]. We chose to extract a slice with a thickness of 60 cm starting at 100 cm above ground level. The idea is to have a slice with a sufficient thickness where all stems with a DBH equal or greater than 5 cm are present (**Fig. 4c**).

We can now use the previously generated slice to obtain the position of the stems in that plot using the plugin `Create 2D Positions From Point Density`. By this we calculate a point density raster. All high-density points above a given threshhold are grouped and used to calculate position of the stems. The main assumption behind this is that the highest verticaly accumulated density of points contained in that slice correspond to trunks. This is a very importand step for detecting stems and the resolution of the density raster needs to be calibrated with respect to the desired tree DBH. With a trial and error approach and due to the fact that our input clouds had an overall very high density a relative threshholding was sufficient for trees with a DBH of 5 cm up to the largest DBH of 135 cm.

Next we defined a point voxel grid (`Create Point Voxel Grid`) using the stem positions obtained in the previous step.The crucial parameter of this step is the minum size of a cubic point group assignable to a tree. If the size of that grid is set to high neighbouring trees might be included due possible overlap of branches between individuals. On the other hand a small grid size would lead to a premature stop of the segmentation process. We found that a value of 8 cm is sufficient for our plot and tree species.

Those stem position need to be translated into so called seed points. A seed point in that context is the starting position for the automatic segmentation process. To create the seed points we use the 2D positions and the previously described 3D point voxel grids to create a three dimensional seed voxel grid using the plugin `Create Seed Voxel Grid`. With those

informations a segmentation voxel grid is created for each tree with a sarting point at 1.3 m above the DTM (**Fig. 4d**).

Now the segmentation process into individual point clouds can take place (`Segmentation Using Seed Voxel Grid`). In principle it combines the 2D positions, the point voxel grids and the seed voxel grid to create a neighborhood topological relationship between the grid cells containing tree points. In essence the cubic grid starting at the stem position in 1.3 m height is moving in z, x and y direction and concatenates those grids which contain points of one tree into a individual cluster per tree. Basically the algorythm determines which point is not yet assigned to a cluster and then checks which cluster is the nearest among the search parameters. This cluster is then defined as the topological parent for that point and is then assigned to the tree cluster. It is important to mention that the cluster is moving first upwards and then downwards (**Fig. 5a**).

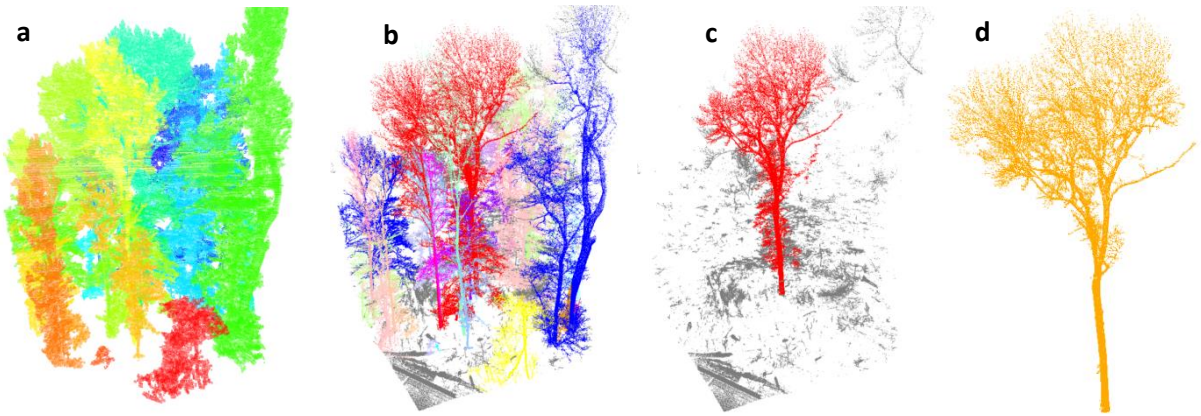

Fig. 5: a) A visual representation of the segmentation grid after the segmentation process. Different colors represent different tree cluster. **b**) Segmented point cloud, different colors represent different tree individuals. The target tree is colored in red. Grey points are not assigned to a tree cluster. **c**) Target tree before manual modification of the segmentation process. **d**) Final segmented tree point cloud.

To manually controll for possible segmentation errors we implemented a modification step plugin called `Modify Voxel Grid Segmentation` provided by the Computree software. In this step we where able to inspect the segmentation process visually (**Fig. 5b**) in a 3D environment. If necessary any falsely assigned points of the target tree could be reassigned by a simple point and click precedure. Every detected tree is represented with a differenet colour and points which were not assigned to any tree cluser are shown in grey. Thus, it was possible to detect branches which were mistakenly assigned due to possible occlusion and reassign those points to the target tree cluster. After the tree cluster was reviewed we veryfied the cluster (**Fig. 5b**, **c**).

With this corrected and verified segmentation grid the segmentation could take place and a individual tree cloud containing only points of the target tree was created. This point cloud was then exported as `ASCII` formated file containing easting, northing and height informations (**Fig. 5d**).

A visual representation of every segmented individal is shown in **Fig. 6**.

Fig. 6: The site of the Leipzig Canopy Crane (LLC) with all segmented tree individuals. Color coding: brown = *C. betulus*, orange = *T. cordata*, blue = *A. platanoides,* violet = *Q. robur*, green = *A. pseudoplatanus*, red = *F. excelsior.*

2.5. Calculation of Quantitative Structure Models

Quantitative Structure Models (QSM) can produce important tree characteristics. As precondition to this point clouds with good quality are necessary. Therefore, we decided to reduce outlier points in the canopy. We developed a batch script which uses the `Statistical Outlier Removal` filter provided by CloudCompare. This filter computes in a first step the average distance of each point to its neighbours [60]. We chose to check for eight neighbours. In a second step it rejects all points that are farther away than the average distance plus two times the standard deviation.[61]

By using this filter we ensured that points recorded during movement due to possible wind are excluded and small branches were preserved and computed correctly, even though some small branchens of large trees might loose some points (compare **Fig. 7 a** and **b**).

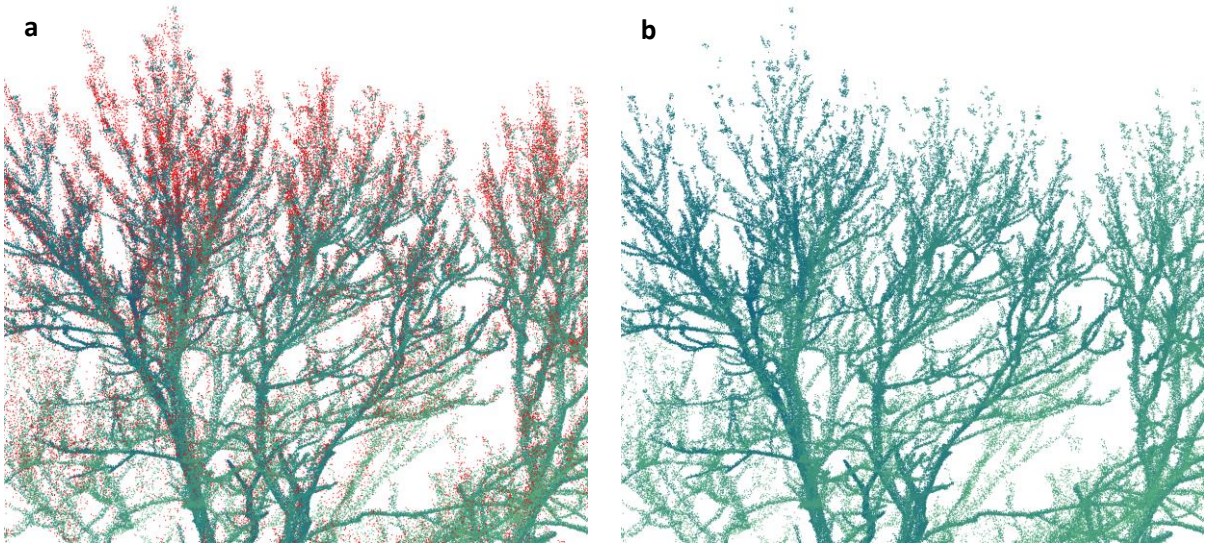

Fig. 7: Visual representation of a part of a tree canopy (*F. excelsior*). **a**) Combination of unfiltered (red) and filtered (blue to green) point cloud. **b**) Filtered point cloud.

The topological reconstruction of the branching structure is the second step. For this we used a MatLab (v. R2018b) plugin developed by Raumonen [45] where the tree point cloud is segmented into stem and individual branches. At this point small patches or subsets of the point cloud, called cover sets (**Fig. 8**) are created using a uniform Voronoi tesselation. Those cover sets are the smallest unit with neighbour relations.

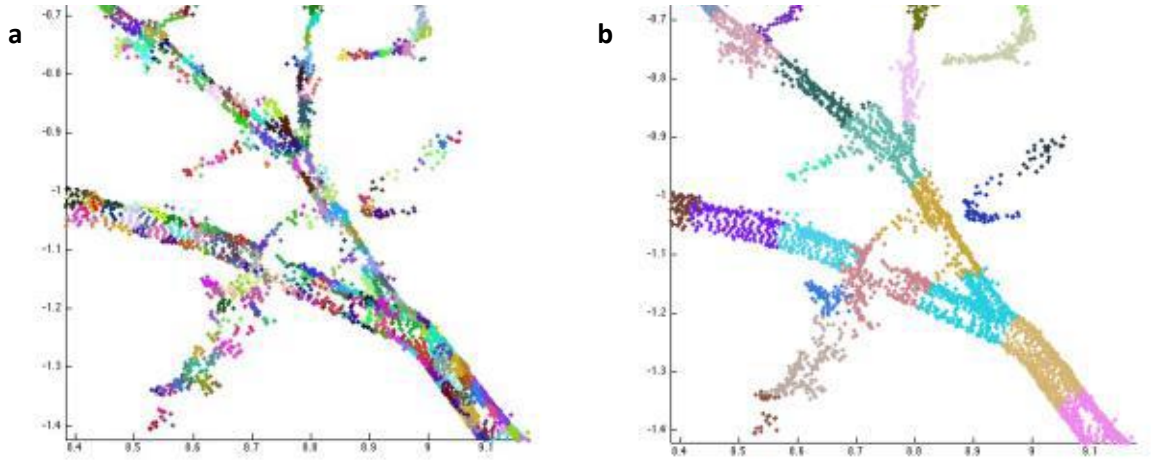

Fig. 8: Comparison of the coves of a branch. In this example the minimum diameters (**`PatchDiam`**) of the cover sets are 2 cm **a**) and 10 cm **b**): Modified picture from `TreeQSM` documentation [62].

It is important to mention one crucial input parameter called `PatchDiam`. This parameter controls the size of the cover sets. On the one hand, smaller cover sets (**Fig. 8a**) capture more details but can lead to disconected point clouds. On the other hand, larger cover sets (**Fig. 8b**) produce point cloud with a greater connectivity with the downside of loosing details. We decided to use `PatchDiam` size of three and five.

In some cases the point cloud might show gaps due to occlusion or the denoising routine. As a result some parts are not connected through neighbour relations due to a small `PatchDiam` size. The algorithm tries to close those gaps using a surface growing method and the neighbour relations are updated. Using this, the next step is the segmentation of the point cloud into parts which have no bifurcations and additionally detect bifurcations. In doing so, different branch orders and therefore as well the stem are segmented (**Fig. 9a**).

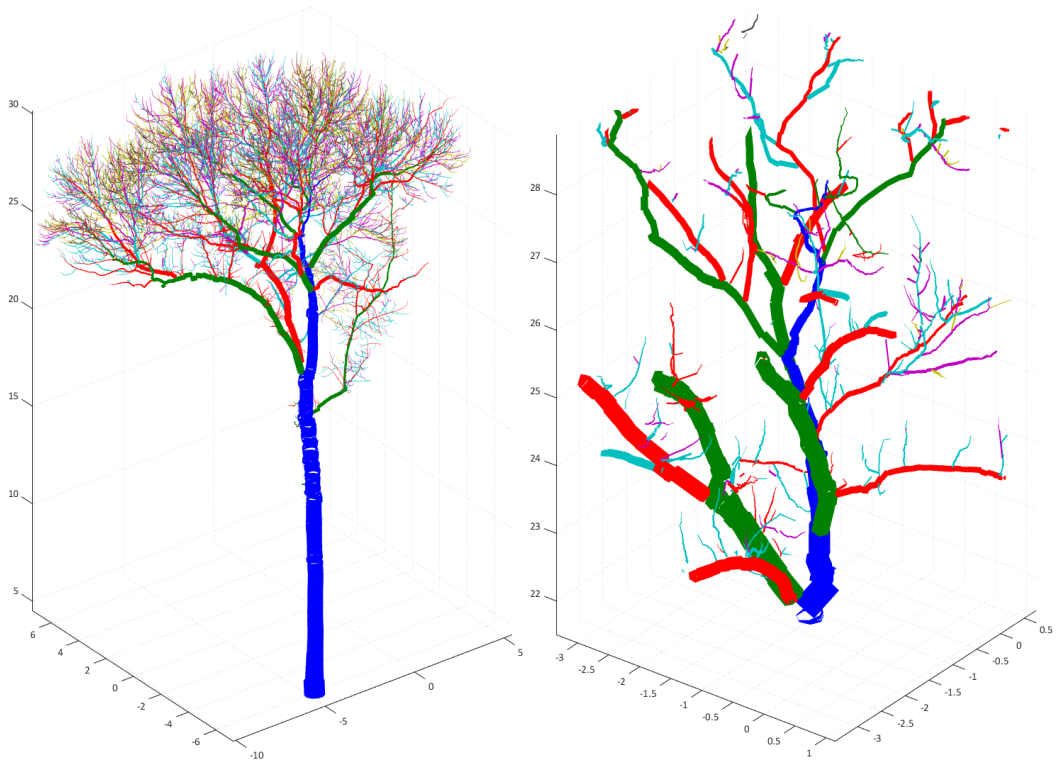

Fig. 9: Visual representation of a hierarchical cylindrical quantitative structure model (QSM). Different colors represent different branch orders. The stem is colored in blue, branch order one in green, branch order two in red and so on.

The third step of the quantitative structure model computation is the geometrical reconstrucion of branch surfaces. With the segmented point cloud we cannot calculate any structural attributes. In order to do this the MatLab function fits basic geometric shapes into these segments **Fig. 9b**.

Since some of the used parameters of the cover set creation are randomly generated we chose to compute four quantitative structure models for every `PatchDiam` size. Therefore, eight data files per tree were created. All computations were executed using a 32-core Intel Xeon CPU E5-2643 0 @ 3.30 GHz with 64 GB of RAM.

In summary we segmented and computed 132 quantitative structure models of *A. platanoides,* 102 of *T. Cordata,* 97 of *F. excelsior*, *61* of *A. pseudoplatanus,* 60 of *C. betulus* and 12 of *Q. robur* summing up to a total amount of 464 tree individuals.

2.6. Additional Structural Analysis using QSM and Real Measurements

In addition to the tree surface area and tree volume we extracted structural information regarding the diameter of the terminal branches of each specie using the quantitative structure models. We randomly selected 20 individuals from each species, except for *Q. robur* were only twelve individuals were available. We wrote a R-Script to extract the diameter of the terminal branches from each of the eight hierarchical ordered cylinder data sets per tree individual. The mean diameter for each individual was plotted as a boxplot.

Furhtermore we measured the diameater on real tree individuals of at least ten terminal branches of one individual per tree species. These measurements were plotted as a boxplot.

Moreover we extracted the total branch number for each individual from the data provided through the quantitative structure model. We then subsampled the dataset to select only those trees which are more or less comparable in their D^2H and therefore are of same age and height. The threshold for the subseting were set to a D^2H ranging from 0.7 to 1.3 m^3, resulting in a data set which contains trees with a height from 16 to 25 m and and diameter at breast height ranging from 17 to 27 cm. We plotted the total number of branches as a boxplot.

2.7. Statistical Analyisis

For handling the huge amount of data (4.14 GB of csv files) we decided to use R (v. 3.6.1) in combination with the R-Studio Software (v. 1.2.1335) for data management and analysis.[63] We developed a script which imported for every tree the extracted structural parameters DBH, height, volume and surface area. In a first attempt to linearize the allometric relationships between volume or surface on the one hand and the linear parameters, DBH and height, on the other hand we used the following formula (**3**) [64].

$$D^2H = DBH \times height \quad \textbf{(3)}$$

Following that we transformed D^2H as well as the volume and tree surface area by means of the natural logarithm to normalize the model residuals. To analyze the relationship

between volume and surface area in respect to D^2H we calculated a linear model, where the response variable is volume or area and the explanatory variable is D^2H and the categorial variable species. A model selection was performed to compare the full ANCOVA model (including species, D^2H and their interaction) against a reduced ANCOVA model (including species effect only), which assumes that every species has the same slope. For model comparison we used the Akaike's "Information Criterion" (AIC).[65] In order to test the differences between every species we developed a loop which replaces the reference species in every iteration.

To further explain potential species differences with respect to surface area we modeled the intercepts resulting from the reduced ANCOVA model against the mean terminal branch diameters measured as stated in 2.6 and presented in **Fig. 11.**

2.8. Calculation of Surface and Volume Allometries

Allometry tries to explain the proportional change of a biological size variable (surface, volume) in respect to a different dimensional attribute of the same individual during organismal growth. Basically, it assumes a relationship between two attributes in the form of a power law equation (**4**).

$$y = ax^b, \quad \textbf{(4)}$$

whereas a and b are constants. The variables x and y represent the aforementioned different dimensional characteristics. More specifically, the constant b is determined by the relative growth rates of the two traits represented by x and y.With this in mind we can use the slope for the constant b and the intercept for the constant a. The variable x is represented by our explanatory variable D^2H.

In order to create linear regression we need to logarithmise equation (**4**).

$$ln(y) = ln\left(ax^b\right) \quad \textbf{(5)}$$

$$ln(y) = ln(a) + ln\left(x^b\right) \quad \textbf{(6)}$$

$$ln(y) = ln(a) + b\ ln(x) \quad \textbf{(7)}$$

We have to raise the intercept a to the power of e in order to reverse the natural logarithm we used to linearize the DBH and Area (**8**).

$$y = e^{a_j} x^{b_j} \quad \textbf{(8)}$$

Whereas j represents the species specific intercept and slope. More easely expressed we can formulate for the surface area (**9**).

$$Area_j = e^{intercept_{area_j}} \times D2H^{slope_{area_j}} \quad \textbf{(9)}$$

With this equation we are able to calculate the surfaca area and volume of six different european tree species using the measured height and DBH in m.

3. Results

3.1. Segmenation and Computation of QSM's

The whole Leipzig Canopy Crane research area includes about 800 tree individuals from 15 different species. As mentioned earlier only trees with a DBH larger than 5 cm were segmented. In some cases a segmentation of the target tree was unsuccessfull and those trees were then excluded as well. A detailed summary of the segmented individuals can be found in **Tab. 2**. Differences from the above mentioned DBH threshhold of 5 cm in the table are due to the least square fitting routine versus the manually measurements of the plot inventory.

Tab. 2: Summary of segmented trees with frequency (n) minimum DBH (Min DBH), maximum DBH (Max DBH), minimum height (Min Height) and maximum height (Max Height).

Species	n	Min DBH [cm]	Max DBH [cm]	Min Height [m]	Max Height [m]
Carpinus betulus	60	3.98	58.52	2.92	31.56
Tilia cordata	102	2.84	83.91	3.58	32.44
Acer platanoides	132	3.32	83.1	5.08	33.47
Quercus robur	12	24.37	135.76	20.39	36.91
Acer pseudoplatanus	61	2.53	39.38	3.62	26.23
Fraxinus excelsior	97	4.72	100.66	7.24	35.33

In total we segmented 60 individuals of *C. betulus* with a DBH range from 3.95 cm to 58.52 cm and a height range from 2.92 m to 31.56 m. Accordingly 102 individuals of *T. cordata* were segmented with a DBH range of 2.84 cm to 83.91 cm and a height ranging from 3.58 m to 32.44 m. 102 individuals of *A. platanoides* were segmented including individuals with a minumum DBH of 2.53 cm and a maximum DBH of 39.38 cm and a height range from 3.62 m to 26.23 m, repectively. In contrast, only 12 individuals of *Q. robur* were segmented with a DBH ranging from 24.37 cm to 135.76 cm and a height from 20.39 m to 36.91 m.

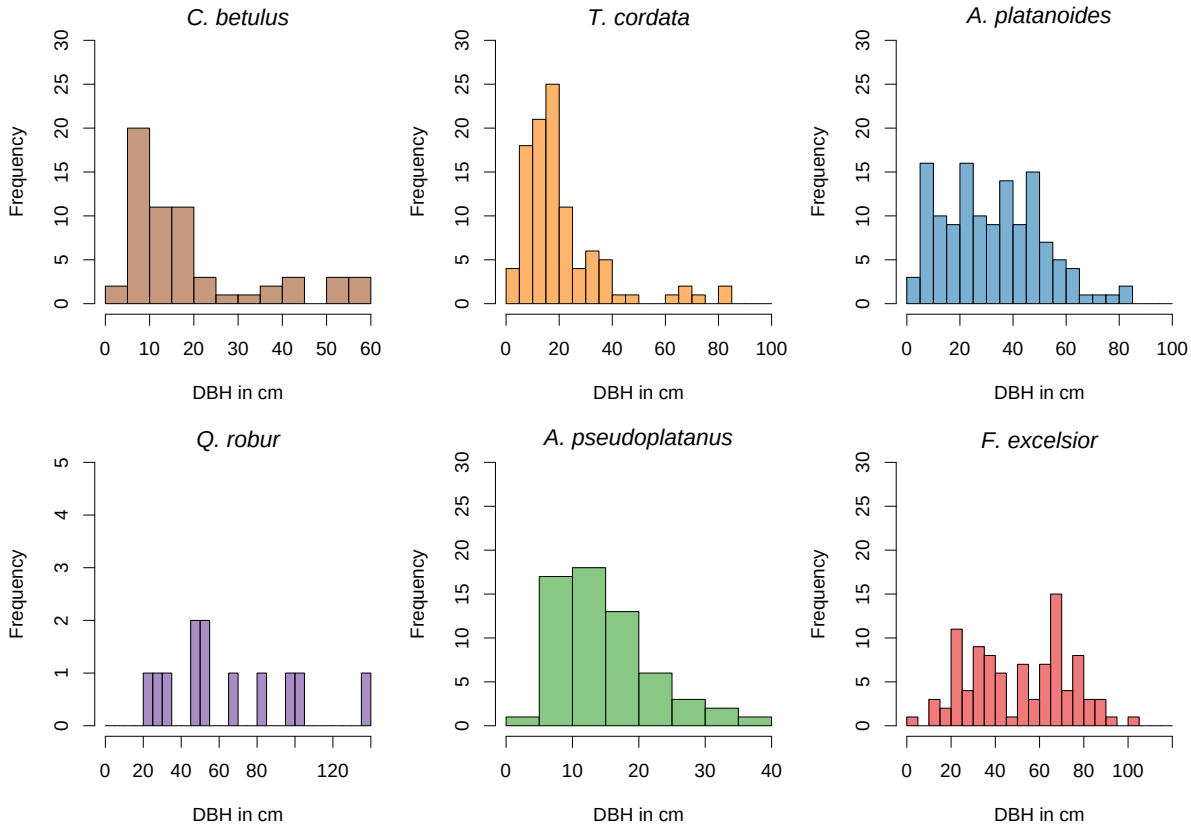

Fig. 10: DBH distributions of the segmented tree species.

The DBH range of the 61 individuals of *A.pseudoplatanus* was 2.53 cm to 39.38 cm with a height range of 3.62 m to 26.23 m. At last we segmented 97 individuals of *F. excelsior* with a DBH range of 4.72 cm to 100.66 cm and a height ranging from 7.24 m to 35.33 m. The DBH distribution for all species is visualized in **Fig. 10**.

3.1. Explaining the Species Effect on Tree Surface Area

As stated in section 2.6 we plotted the mean diameter of the terminal branch of the species as a boxplot. Those diameters are shown in **Fig. 11**. In the left hand plot the mean diameter of the extracted structural informations of the quantitative structure models were used. In the right hand plot the measured diameters in the *Leipzig Canopy Crane (LLC)* research area were plotted. Using the measured values, *C. betulus* shows the smallest terminal branch diameter with a mean of 1.3 mm. The mean diameter of *T. cordata* is 2.9 mm. Followed by *Q. robur* with a mean diameter of 3.4 mm. *A. platanoides* has a mean terminal branch diameter of 4.3 mm and *A. pseudoplatanus* of 5 mm. In contrast, *F. excelsior* has a mean terminal branch diameter of 5.3 mm. The extracted diameters of the quantitative structure model are slightly overestimated. The overall relationship still remains

the same, for instance *F. excelsior* still is represented with the largest terminal branch diameter and *C. betulus* with the smallest.

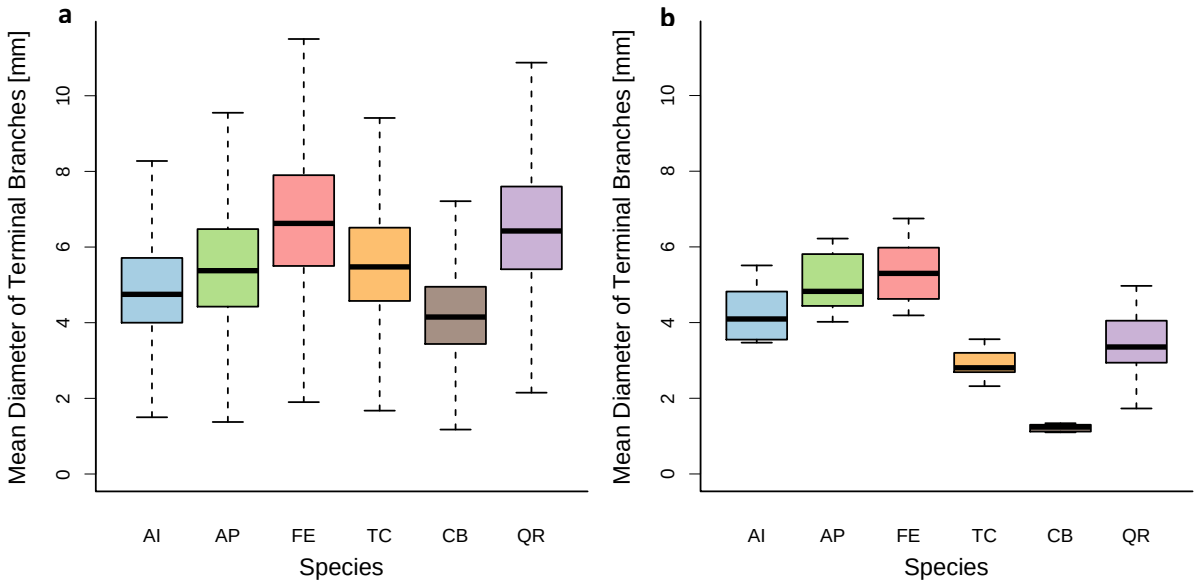

Fig. 11: a) Boxplot of mean the measured diameter of the last branch of different species in mm. **b**) Mean diameter of the last branches of 20 individuals per species calculated with the QSM. The whiskers represent the 25th and 75th quartile of the measured data. AI = *A. platanoides*, AP = *A. platanoides*, FE = *F. excelsior,* TI = *T. cordata*, CB = *C. betulus*, QR = *Q. robur*.

With the mean terminal branch diameters for each species we calculated a linear ANCOVA model which uses the coefficients calculated by the ANCOVA model for the tree surface area. Basically, we want to test if we find a correlation between terminal branch size and surface area. This model tests the relationship between terminal branch diameter and tree surface area. **Tab. 3** shows the summary of the linear model regarding the terminal branch diameter correlated with the coefficients of the ANCOVA model for the tree surface area. The R^2 value of 0.8621 indicates that the model explains the relationship between those two traits well. As well the p-value is considered significant. The intercept with the y-axis is 5.0524 and the slope is -0-2817. This relationship is visualized in **Fig. 12a**. The black regression line shows a clear negative relationship between the terminal breach diameter and the regression coefficients of the tree surface area. Those findings indicate that the larger the terminal branch diameter is, the smaller is the tree surface area and vice versa.

In Fig. **12b** we plotted the total branch number in a boxplot. We show here that trees with a small terminal branch diameter like *C. betulus* and *T. cordata* have more bifurcations, expressed in a higher total number of branches. Thus, indicating that species-specific traits like the terminal branch diameter do influence tree surface area. In this subset containing *C. betulus* individuals with a diameter at breast height range of 17 to 27 cm have a mean

branch number of roughly 4000 compared with *F. excelsior* with the same diameter at breast height range containing approximately 650 branches.

Tab. 3: Summary table of the linear model of terminal branch diameter and the coefficients calculated with the restricted ANCOVA model for the tree surface. The standard error is given in brackets

	Branch diameter
Target	**Regression coefficients**
Intercept	5.0524 (0.221)
t-value	22.804
Slope	-0.2817 (0.0563)
t-value	-5.002
Res. Std. Error	0.1915 DF = 4
Mult. R^2	0.8621
Adj. R^2	0.8277
F-Statistic	25.02 DF = 1 and 4
p-Value	0.0074

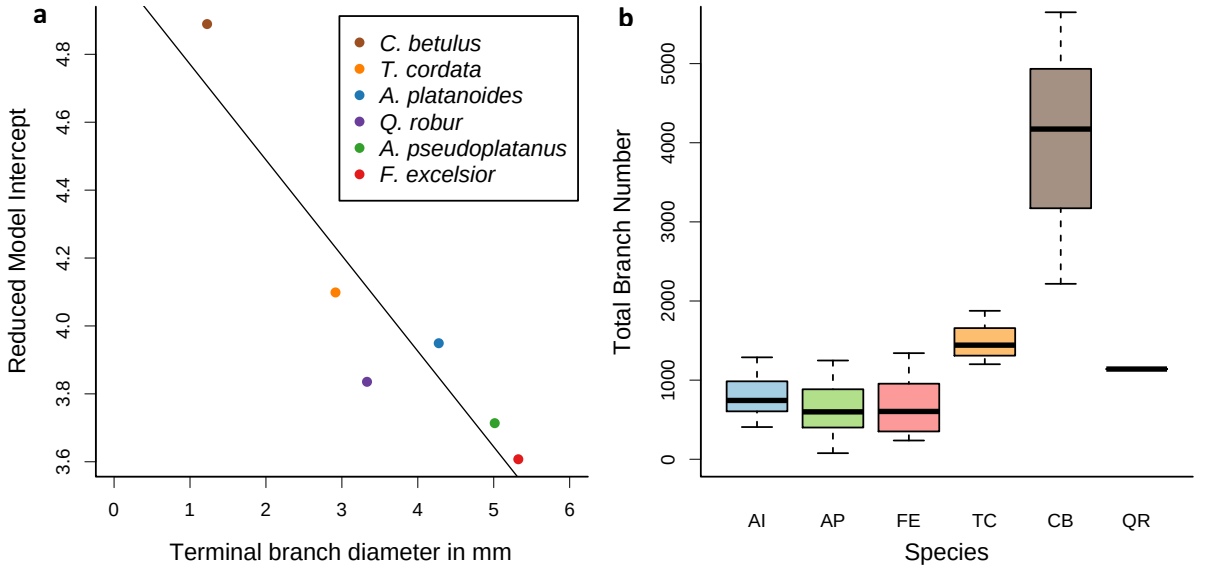

Fig. 12: a) Visual representation of the terminal branch diameter of the six species plotted against the regression coefficients calculated with the restricted ANCOVA linear model of the tree surface area. **b**) Boxplot of total branch number of tree species of approximately the same D^2H. AI = *A. platanoides*, AP = *A. platanoides*, FE = *F. excelsior,* TI = *T. cordata*, CB = *C. betulus*, QR = *Q. robur.*

3.2. Explaining the relationship of Surface Area, Volume with Tree Architecture

For a better understanding of the allometric relations of tree surface area and volume in respect to D^2H we created two plots for each attribute (**Fig. 13**). These figures suggest that

C. betulus has the largest surface area followed by *T. cordata*, while *F. excelsior* exhibits the smallest surface area. The different slopes and intercepts are displayed in **Tab. 4**.

As mentioned in 2.7 we calculated a full linear model and a reduced ANCOVA modell assuming that every species has the same slope. The AIC for the first model was 350.99. The AIC for the second model was 341.96. For further analysis, we used the reduced ANCOVA modell applying the principle of parsimony. Therefore, the slopes regarding the tree surface area were treated as equal between species (**Tab. 4**). In **Tab. 5** we report the significance levels of the ANCOVA comparisons of the species regarding their intercepts. As shown in **Fig. 13a** there was a significant difference ($p < .001$) in the intercepts calculated for the tree surface area for all species compared with *C. betulus*. Statistical significance between the intercepts of *T. cordata* versus *A. platanoides* ($p = .008$), *Q. robur* ($p = .017$), *A. platanoides* and *F. excelsior* ($p < .001$) was determined.

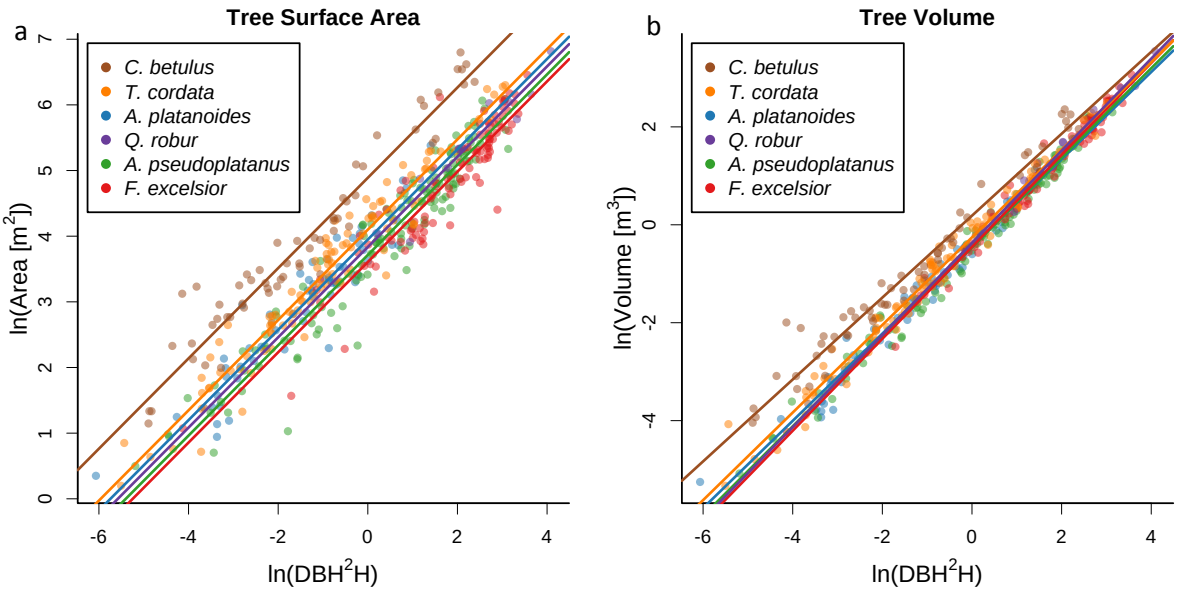

Fig. 13: Scatterplots of tree surface area (a) and tree volume (b). Different colored dots and lines correspond to different species. The x-axis is showing the natural logarithms of the squared DBH multiplied with the tree height (D2H). The y-axis represents the natural logarithm of the area (a) respectively of the volume (b).

Results were considered significant for *A. platanoides* versus *A. pseudoplatanus* and *F. excelsior* ($p < .001$). There was no statistical difference between *A. platanoides* and *Q. robur* ($p = .322$). In contrast *Q. robur* showed significant differences in the intercepts compared with *A. pseudoplatanus* and *F. excelsior* ($p < .001$). Regarding *A. pseudoplatanus* compared with *F. excelsior* we found a statistical difference in the intercept ($p = .028$). Regarding the tree volume, we modeled a full and a reduced ANCOVA model. The AIC of the

reduced model was -28.56. Compared to the full model with an AIC of -45.14 which was thus chosen as the final model.

Tab. 4: Summary of the statistics with intercepts and slopes for the different species regarding the tree surface area and tree volume. DF = degrees of freedom, Significance levels: * p = 0.05, ** p = 0.01, *** p = 0.001

	Tree Surface Area					
Species	***C. betulus***	***T. cordata***	***A. platanoides***	***Q. robur***	***A. pseudoplatanus***	***F. excelsior***
Intercept	4.8891	4.0987	3.9491	3.8355	3.7136	3.6074
Std. Error	0.0468	0.0354	0.0463	0.1023	0.0304	0.0389
t-value	104.504	115.847	85.368	37.507	122.305	92.805
p-value	***	***	***	***	***	***
Slope	0.6877					
Std. Error	0.0094					
t-value	72.884					
p-value	***					
Res. Std. Error	0.3464 DF = 457					
Mult. R^2	0.9369					
Adj. R^2	0.9361					
F-Statistic	1131 DF = 6 and 457					

	Tree Volume					
Species	***C. betulus***	***T. cordata***	***A. platanoides***	***Q. robur***	***A. pseudoplatanus***	***F. excelsior***
Intercept	0.1863	-0.2569	-0.4418	-0.3689	-0.4591	-0.4499
Std. Error	0.361	0.0255	0.0404	0.1482	0.0202	0.0383
t-value	5.169	-10.762	-10.929	-2.490	-22.749	-11.743
p-value	***	***	**	*	***	***
Slope	0.8365	0.8945	0.8901	0.9407	0.9142	0.9391
Std. Error	0.0144	0.0123	0.0202	0.0587	0.0108	0.0175
t-value	57.996	72.984	44.152	16.016	85.026	53.807
p-value	***	***	**	***	***	***
Res. Std. Error	0.2271 DF = 452					
Mult. R^2	0.9853					
Adj. R^2	0.985					
F-Statistic	2762 DF = 11 and 452					

In **Fig. 13b** it can be seen that the slope of *C. betulus* is in fact less steep compared to other species. This is shown as well in **Tab. 4** were every species has its own slope. In addtion, only *C. betulus* is showing the highest intercept value followed by *T. cordata*. In **Tab. 5** we present the significance levels for the tree volume. The intercepts are significantly different for *C. betulus* compared to the other five species ($p < .001$). *T. cordata* showed no

significant difference compared with *Q. robur* (p = .863). *T. cordata* compared with *A. platanoides*, *A. pseudoplatanus* and *F. excelsior* showed a statistical significance difference (p < .001 respectively p = .001).There was no statistical difference between *A. platanoides, A. pseudoplatanus* and *F. excelsior* (p = .631 and p = .136). We found a slight significant difference between *Q. robur* versus *A. platanoides* (p = .032) and *A. pseudoplatanus* (p = .001) respectively. No significant difference could be found between *F. excelsior* and *Q. robur* (p = 0.136). In contrast a significant difference was detected between *F. excelsior* and *A. pseudoplatanus* (p = .017).

Tab. 5: Significance levels of the intercepts of tree surface area and volume. The abbreviations stand for: CB = *C. betulus*, TI = *T. cordata*, AI = *A. platanoides*, QR = *Q. robur*, AP = *A. platanoides*, FE = *F. excelsior*. Significance levels: * p = 0.05, ** p = 0.01, *** p = 0.001

	Tree Surface Area						**Tree Volume**					
	CB	***TC***	***AI***	***QR***	***AP***	***FE***	***CB***	***TI***	***AI***	***QR***	***AP***	***FE***
CB		***	***	***	***	***						
TC			**	*	***	***	***					
AI				n.s.	***	***	***	***				
QR					***	***	***	n.s.	*			
AP						*	***	***	n.s.	***		
FE							***	***	n.s.	n.s.	*	

These findings suggest we have an effect on species on area and volume.

3.3. Calculation of Allometric Coefficients

Our findings of the linear regression show a clear dependency between diameter at breast height and height with tree surface area and tree volume. One can use those coefficients to calculate the area and volume using only the diameter at breast height and height of a tree. With the formula (**9**) stated in section 2.8 we will now give an example how to calculate the area (A) and volume (V) of an fictive indiviudual of *T. cordata*. We used the intercept and slope provided in **Tab. 4** with a height of 18 m and a DBH of 0,15 m.

$$A_{Tilia} = e^{intercept_A} \times D^2H^{slope_A} \qquad V_{Tilia} = e^{intercept_V} \times D^2H^{slope_V} \quad \textbf{(10)}$$

$$A_{Tilia} = e^{4.1018} \times (0.15^2 \times 18)^{0.6877} \qquad V_{Tilia} = e^{-0.2569} \times (0.15^2 \times 18)^{0.8945} \quad \textbf{(11)}$$

$$A_{Tilia} = 32.47\ m^2 \qquad V_{Tilia} = 0.34\ m^3 \quad \textbf{(12)}$$

Whereas, e is the euler number, D^2H represents the squared diameter at breast height multiplied with tree height. The $intercept$ is the intercept calculated with the linear models

for tree surface and volume against D^2H and the $slope$ from the same models. Those calculations are in agreement with the data we computed with the quantitative structure models.

The allometric equation (**9**) regarding the tree surface area can further be simplified if we implement our finding, that the slopes do not differ between species, into our equation.

$$Area_j = e^{intercept_{area_j}} \times D2H^{slope_{area_j}} \quad \textbf{(13)}$$

This leads us to the following equation (**14**):

$$Area_j = e^{intercept_{area_j}} \times D2H^{slope_{area}} \quad \textbf{(14)}$$

Using this equation we still need a calculated intercept for a specific species. Therefore, we cannot calculate the tree surface area of an unknown tree species. If we use our finding presented in section 3.1 of the terminal branch diameter effect on the surface area we can further modify the allometric equation as following (**15**):

$$Area = e^{m \times TBD + n} \times D^2H^l \quad \textbf{(15)}$$

Whereas m and n represents the slope or respectively the intercept of the regression of the terminal branch diameter and the tree surface area model presented in **Tab. 3** and l represents the slope calculated for tree surface area against D^2H presented in **Tab 4**.

4. Discussion

4.1. Modeling and Allometric Equations

In total 464 tree individuals were used to build QSM's. With those we were able to plot and calculate linear models of the calculated tree surface area and the tree volume (**Fig. 13**).Those models had an adjusted R^2 value ranging from .864 to .941. Therefore, the precision of the model was rated high for each model although, scattering of the measurement values were visible in the plots. Furthermore, we found significantly different (**Tab. 5**) intercepts presented in **Tab. 4** for the tree surface area and tree volume at a given combination of diameter and height. As presented in **Fig. 13** *C. betulus* has the largest tree surface area and tree volume. These differences are significant compared to all other species ($p = <.001$). The smallest surface area was calculated for *F. excelsior*. The mechanism underlying the variation of surface area und volume can be explained with the help of the Corner's rule. [29–31] This theorem postulates that the twig size is positively correlated with

the appendages, namely the leaves.[66] Bigger, or for that matter, heavier leaves are positively correlated with larger diameters of the terminal twigs.[29–31] In **Fig. 11** the terminal branch diameter are presented as a boxplot. The smallest terminal branch diameter was measured for *C. betulus*. In addition, the largest tree surface area and the largest tree volume was calculated for *C. betulus* using the quantitative structure models. Those findings suggest that the available tree surface area is correlated with other architectural traits. For example, branch diameter, bifurcation patterns and leave sizes. In contrast, the largest terminal branch diameter was measured for *F. excelsior*. In accordance, the available surface area and volume was the smallest.

To describe the relationship between twig diameter and twig surface we can use in a first approximation the basic geometrical shape of a cylinder. If adjacent segments of a cylinder are divided into progressively smaller branches, the surface area increases with the number of terminal branches which in turn is inversely proportional to their diameter. In other words, the diameter is a proxy for the branching intensity and with this a useful predictor of surface area at a given volume of the cylinder.

The main reason for the increase of surface area with a decreasing terminal twig diameter might be that trees with larger terminal branch diameters have fewer bifurcations and branches this fact is shown in **Fig. 12b**. This might be due to the fact that a thick twig with large or heavy leaves weights more than a smaller twig. As well since terminal twig diameter is positively correlated with leave size [29–31] we showed that trees with small diameters have more twigs. Thin twigs support only small leaves and the tree has to compensate leave area for photosynthesis with more leaves compared with a tree with large leaves.

In addition to our findings of the relationship between tree surface area and D^2H, we investigated if we find a correlation between terminal branch diameter and the tree surface area. In **Fig. 12a** and **Tab. 3** we present a model which shows a clear correlation between those two traits. The statistically significant negative relationship between terminal tree branch diameter and the tree surface area implies that trees species with small terminal branch diameters have a significant larger surface area compared with species having larger terminal branch diameters. Not only can we use this to explain why different species have different surface areas we can now use this relationship to calculate the area of tree species which we haven't focused on in this thesis. Therefore, we need to introduce a third

measured parameter, namely the mean terminal branch diameter, in addition to height and DBH to calculate the tree surface area.

Regarding the tree volume we found as well statically significant differences between the slopes and intercepts of the different species (Tab. 5). Those differences where in general less significant, implying that the tree volume is not as strongly influenced by species or terminal branch size. It is important to understand that the area is a function of the volume. With this in mind, we can understand how trees allocate carbon in respect to leave size [67] and therefore twig size. Basically, the allocated volume remains the same in respect to DBH and tree height. Only the tree surface area changes due to the fact of different bifurcation patterns and allocation of carbon into the branches.

4.2. Study Site, Data Collection and Point Cloud Preparation

By scanning the whole plot using TLS we had a suffiently large sample size for at least six tree species to compute tree specific attributes. The scans needed to be of good quality. Therefore, we decided to at the end of march to avoid occlusion through leaves. Secondly, scans were taken with almost no wind. This is important, because the wind is interacting with twigs and branches in the canopies resulting in movement. This could lead to falsely recorded points reducing the accuracy of the scan and hence the resulting QSM. Overall, the scan quality was very good with no occlusions or movement artifacts, with few exceptions in the upper part of tree crowns (**Fig. 7**). This is due to the very dense scanning grid we used. This way we ensured a very good cover of stems as well of the upper parts of canopies. To improve the cover of higher tree canopies one could scan the canopies from above using a tower, like the one availiable for FARO Laser Scanner Focus^{3D}. In addition, the resolution of the scan decreases with the distance due to the angular azimut. Leading to an overestimation of small twig diameters (compare **Fig. 11a** and **b**). This can result in a overestimation of tree surface area and tree volume. The impact of this on our analysis is rated minimal for small trees, but for large trees we can not exclude the possibility that small branches for instance of *C. betulus* in higher canopies are overestimated. Therefore, in future scans in a more dense grid or the above mentioned towers should be used to minimize the effect of a scanning resolution decrease with incraesing distance. Regardless, we had a few cases of movement due to wind resulting in artifacts (**Fig. 14**). In some cases we can not exclude the possibility of uncorrect registrated point clouds. As shown in **Fig. 14**

one can see a shadow-like point cloud right next to a more dense appearing point cloud. We assume this artifact occures after the merging process (explained in 2.3 and visualized in **Fig. 3**).

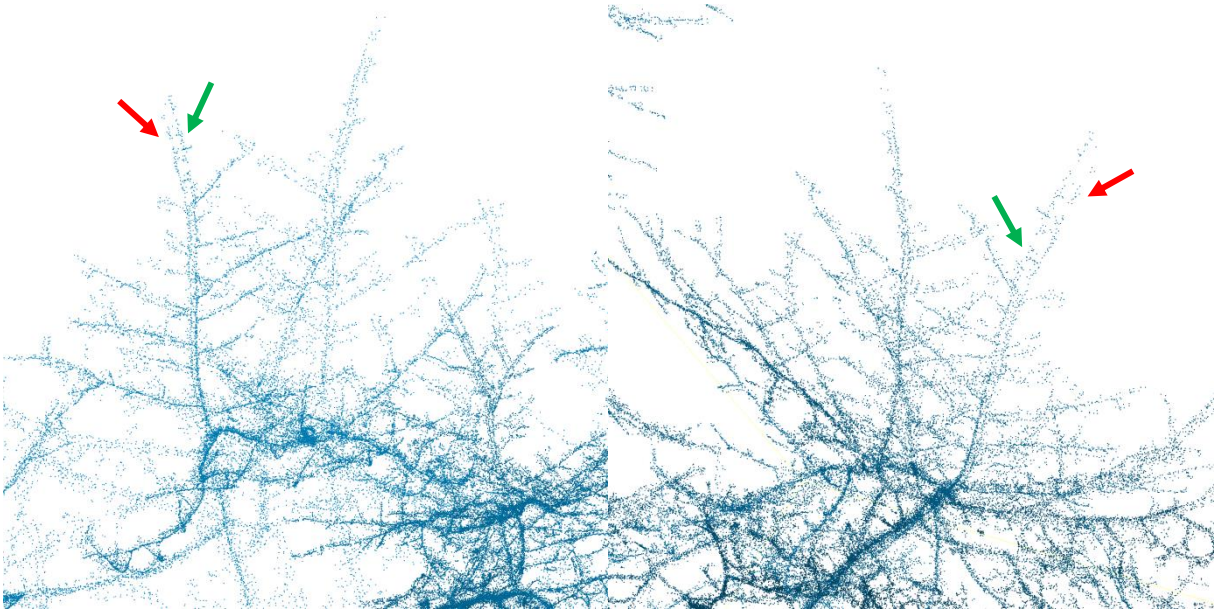

Fig. 14: Capture of the same twig of a *C. betulus* individual from different perspectives showing possible wind or registration artifacts. Red arrow pointing to either the falsely registrated points or points recorded during wind.

One point cloud might contain points which were not correctly registrated. A alternative explanation could be that the tree shifted during the scaning process because of wind. As mentioned above it is also likely that points recorded at a great distance to the target tree might decrease in accuracy. To avoid this we only used point clouds with a minumum size of 4 MB (see chapter 2.3).

Provided with data from a forest inventory in 2015, we used tachymetric measured geo-positions, tree dimensions and species names to identify target trees. Since the inventory took place three years before scanning and analyzing the data some of the old trees were found to be dead and therefore not available for this study. In addition, some of the younger trees in the understory had to be excluded because they were not included originally in the inventory and therefore missing crucial data like position and species. In some cases it was impossible to distinguish between two young and closely situated tree individuals even though using their stem positions. Those individuals were excluded from the segmentation process as well. Having said this, we need to mention that for most of the six species young individuals with a DBH <10 cm were abundantly available and therefore excluding a few of them presents no problem.

4.3. Segmentation into Individual Tree Clouds

Our strategy of segmenting tree clouds resulted in very good quality single tree point clouds with almost no points from the understory, ground or other tree individuals even though some trees were close to each other and some branches overlapped into the canopies of other trees. The use of an automatic approach of creating individual tree clusters (**Fig. 5a**) enabled us to decide easely by visual inspection which cluster belongs to the target tree. With an easy 3D point and click procedure provided by Computree we were able to reassign incorrectly classified clusters in a matter of seconds. However, this procedure stand opposite to fully automatic procedures like the open source software like `treeSEG` [68] and a software developed by Ackerbloom [43]. Those appoaches promise a good segmentation of whole forests without human intervention. `treeSEG` for instance is able to segment a 3.8 GB point cloud with 338 million points containing 155 trees within nine days using a 24-core 2.4 Ghz CPU workingstation. The point clouds comprising only the area with all our target trees with a point density used in this thesis would ammount to a data set with of roughly 60 GB. To process such large data sets we could either downsample our point cloud loosing accuracy and informations or we could subsample the data set into managable sub clouds. In the first cases the processing time would decrease. But eventually the resulting quantitative structure models would not be sufficient to calculate good estimates of allometric coefficents. In the second case, we would maintain the desired point cloud quality but the processing time is very long. In addition, we would have to identify the tree species after the segmentation process using the geo-position of each target tree. Furthermore, from our perspective the segmentational process is not reliable enough to provide point clouds for calculating quality quantitative structure models for allometric estimations. Therefore we stand by our choice to use the semi-automatic approach in order to ensure good single tree point clouds.

4.4. Calculation of Quantitative Structure Models

As of now there are a few methods available to compute QSM. The most prominent are the “sphere-following” method called `SimpleTree` developed by Hackenberg [58] and the “cover set” method called `treeQSM` developed by Raumonen [45,62]. Both methods use basic gemotrical shapes like cylinders to model a tree based on a TLS scan of a tree. In a first approxmimation a tree is constructed like a collection of differently sized cylinders. In

addition, one can easily determine basic informations like shell surface or the volume of a cylinder. Furthermore, it is possible to extract additional information like angular position and bifurcation patterns to calculate other relevant structural data. We decided to use the cover patch method developed for MatLab. This method is generating very good estimations of a TLS scan. [43,44] In contrast to `SimpleTree` even a large `ASCII` formated point cloud with 616 MB containing 9 274 439 points is processed in under 10 minutes compared to couple of hours using `SimpleTree`. Using cylinders as an approximation for the structure of a tree comes with some limitations in accuracy. As shown in **Fig. 9** and **Fig. 15** one can see that the basic shape and structure of the stem is represented very good.

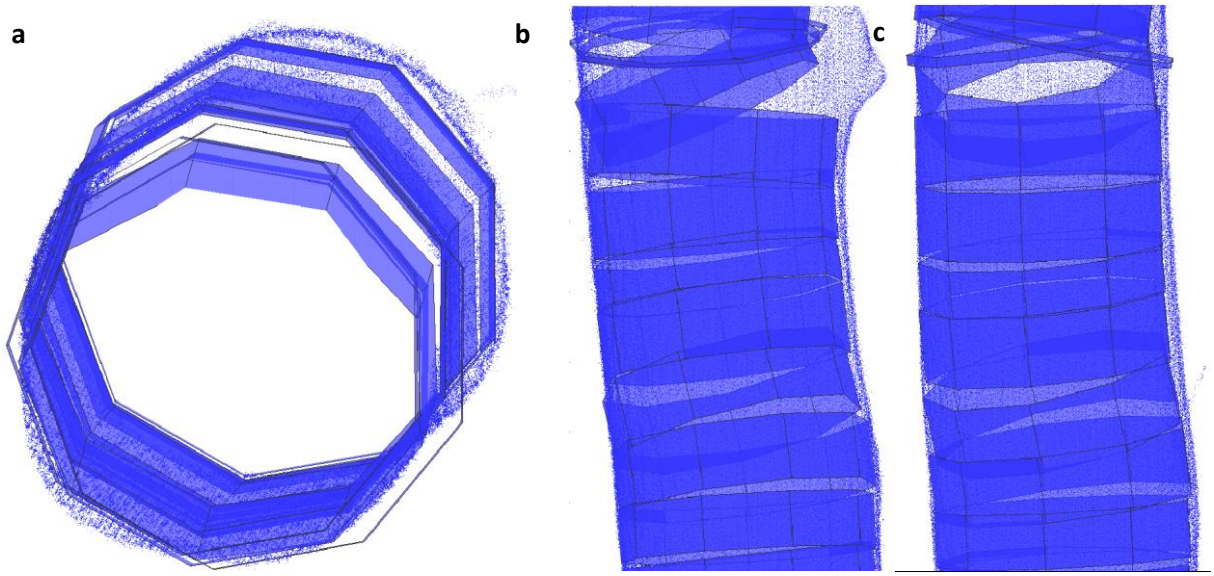

Fig. 15: Close up representation of the stem of an individual of *F. excelsior*. In this figure the fitted cylinder is simplified by a multisided shape. **a**) View from top. **b**) View from the side. **c**) View from the side rotated by 90° in respect to **b**.

Having said that, if we look closely one can see that that a tree cross-section is not a perfect circle. As an effect the real structure could only be modeled using tesselation models. `TreeQSM` is equipped with this function, at least for a trianguled representation of the stem. Though, those information were not used in this thesis.

In addition different species have different bark structures (**Fig. 16**). The bark influences greatly the available surface area [21,22].Recall the bark structure of *F.* excelsior or an old *Q.* robur. Both species have deep furrowed bark. Those furrows can not be modeled with simple geometric shapes. As shown in **Fig. 16b**, a clear discrepancy between the gree cylinder and the outer shell of the bark can be seen.

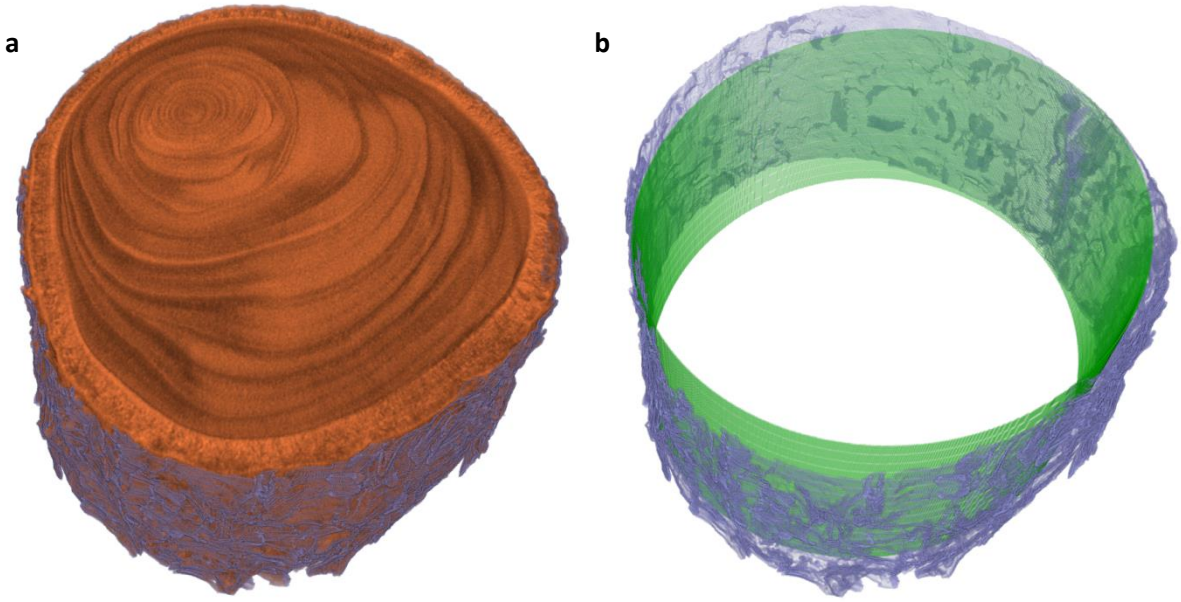

Fig. 16: a) X-Ray computer micro tomography Scan of a 4 cm thick twig of *Pinus nigra*. The bark surface layer was segmented und is here highlighted in violet. **b**) Same surface area with a cylinder (green) fitted into the branch using a least square approach. A clear discrepancy can be seen, as well that the fine furrowed structure is not represented by the cylinder.

In this particular case the difference in the surface area was calculated to be about 50 %. Future studies will have to continue to explore how bark structure influences the available tree surface area. Nonetheless the generated QSMs provide a very good estimation of the segmented trees (**Fig. 9**). We can use those to calculate allometric coefficients.

5. Conclusion

Remote sensing is a fast growing field with a wide application range. In this thesis we used the opportunities namely the accuracy and speed provided by terrestrial laser scans to scan a large scale forest plot. With the high accuracy and quality of the generated point clouds we were able to successfully generate a sufficient amount of highly accurate quantitative structure models of six European tree species using a fast and reliable method.[69] By the means of those models we found out that different tree species have different surface areas whereas the volume is not considerably different. Furthermore we showed that trees with small terminal branch diameter have in general more branches. In addition we present the means to calculate the surface area of six European tree species by using easily obtainable tree characteristic's like DBH and tree height. With additional architectural information, like terminal branch diameter we were able to present a approach to predict the tree surface area even without calculating the allometric dependencies.

6. Appendix

i. CMD script for sub-sectioning the ASCII scan files

```
for /f "usebackQ tokens=1,* delims= " %%i in ("PATH_TO_LIST_OF_VERTICES") do
    call :cropFile %%j
    echo %%*
    echo done
    pause
    exit /b

:cropFile
for %%f in ("F:\03_output") do (
    echo file %%i  ...
    md "%%~f\%%i"
 for %%k in ("PATH_TO_ORIGINAL_SCAN_FILES") do
     for /f "tokens=4 delims=\" %%n IN ("%%k%%") do
         start /w "" "PATH_TO_CLOUDCOMPARE.EXE"
         -SILENT
         -O
         -GLOBAL_SHIFT -312600 -5693000 0 %%k
         -AUTO_SAVE OFF
         -CROP2D z 6 %*
         -C_EXPORT_FMT BIN
         -SAVE_CLOUDS FILE: "OUTPUT_PATH\%%i\%%n"
)
```

ii. CMD script for merging of sub-clouds

```
@echo off

SetLocal ENABLEDELAYEDEXPANSION

  set "originalPath=ORIGINAL_PATH*"

  set "outputPath=OUTPUT_PATH"

  set "programPath=start /w "" "PATH_TO_CLOUDCOMPARE.EXE" -SILENT -C_EXPORT_FMT BIN"

set folderIncrement=0

@echo call :mergeFiles >!outputPath!output.txt

:mergeFiles
for /d %%A in (%originalPath%) do (
    set subFolderPath=%%A\*
    set "filesToMerge="
      echo ----------------------------------------
      echo Merging Files In Folder: ID = "%%~nxA"
      echo ----------------------------------------
      echo +                                      +
    set /A folderIncrement=!folderIncrement!+1
    set fileIncrement=0
    for %%F in (!subFolderPath!) do (
        set fileSize=%%~zF
           if !fileSize! LEQ 255000000 (
              if !fileSize! GEQ 4000000 (
            set fileName=%%~nxA%.bin
            echo - File %%~nxF added to queue
            set "filesToMerge=!filesToMerge! -O %%F"
            set /A fileIncrement=!fileIncrement!+1
              )
           )
        )
    set "saveAllParameter= -SAVE_CLOUDS ALL_AT_ONCE FILE: !outputPath!!fileName!"
```

```
    set "commandLine=%programPath%!filesToMerge!!saveAllParameter!"
    echo +                                        +
    echo[
    echo   ~ Saving File Into Output Directory ~
    echo !outputPath!
    echo[
    !commandLine!
    echo                FINISHED!
    echo[
    echo       - !fileIncrement! Files merged
    echo[
    )
echo ________________________________________
echo ----------------------------------------
echo[
echo          All Folders Processed!
echo           !folderIncrement! Folders Processed!
echo               ==========
ENDLOCAL
goto :eof
          -O
          -GLOBAL_SHIFT -312600 -5693000 0 %%k
          -AUTO_SAVE OFF
          -CROP2D z 6 %*
          -C_EXPORT_FMT BIN
          -SAVE_CLOUDS FILE: "OUTPUT_PATH\%%i\%%n"
)
```

iii. Computree Script summary

```
Num Plugin      Step Name                          Step Description
1   base        PB_StepCreateReaderList            1- Create a list of readers
2   base        PB_StepBeginLoopThroughGroups02    1- Loop on groups
3   base        PB_StepUseReaderToLoadFiles        2- Load file using readers
4   ONF         ONF_StepClassifyGround             Classify ground points (TLS)
5   ONF         ONF_StepComputeDTM02               Create DTM
6   SimpleTree  ST_StepExtactSliceAboveDTM         Smooth extraction of a point slice pa
rallel to the DTM.
7   ONF         ONF_StepExtractPositionsFromDensity Create 2D position from points densit
y
8   ONF         ONF_StepCreatePointGrid            Create point voxel grid
9   ONF         ONF_StepCreateSeedGrid             Create seed voxel grid
10  ONF         ONF_StepSegmentFromSeedGrid        Segment using seed voxel grid
11  ONF         ONF_StepModifyVoxelSegmentation    Modify voxel grid segmentation
12  ONF         ONF_StepExtractPointsFromGrid      Segment a scene using an indice grid

13  ONF         ONF_StepComputeCrownProjection     Horizontal projection of crowns
14  base        PB_XYBExporter                     Points, XYB (X,Y,Z,I)
15  base        GDAL_ESRI_Shapefile                GDAL ESRI Shapefile
16  base        PB_CSVExporter                     Attributes export (csv)
17  base        CT_StepEndLoop                     2- Ends a loop in the script
```

7. Bibliography

References

[1] Malhi, Y., Jackson, T., Patrick Bentley, L., Lau, A., Shenkin, A., Herold, M., Calders, K., Bartholomeus, H. & Disney, M. I. 2018 New perspectives on the ecology of tree structure and tree communities through terrestrial laser scanning. *Interface focus* **8**, 20170052. (doi:10.1098/rsfs.2017.0052).

[2] Leonardo & Richter, J.P. 1970 *The notebooks of Leonardo da Vinci.* New York: Dover.

[3] Shizonaki, K, Yoda, k, Hozumi,K Kira, T. 1964 A quantitative analysis of plant form - the pipe model theory: II. Further evidence of the theory and its application in forest ecology. *Japanese journal of ecology*, 133–139.

[4] Shizonaki, K, Yoda, k, Hozumi,K Kira, T. 1964 A quantitative analysis of plant form-the pipe model theory: I. Basic analyses. *Japanese journal of ecology*, 97–105.

[5] Chiba, Y. 1991 Plant form based on the pipe model theory II. Quantitative analysis of ramification in morphology. *Ecol. Res.* **6**, 21–28. (doi:10.1007/BF02353867).

[6] West, G. B., Brown, J. H. & Enquist, B. J. 1997 A general model for the origin of allometric scaling laws in biology. *Science (New York, N.Y.)* **276**, 122–126. (doi:10.1126/science.276.5309.122).

[7] Enquist, B. J., West, G. B. & Brown, J. H. 2009 Extensions and evaluations of a general quantitative theory of forest structure and dynamics. *Proceedings of the National Academy of Sciences of the United States of America* **106**, 7046–7051. (doi:10.1073/pnas.0812303106).

[8] Stockfors, J. 2000 Temperature variation and distribution of living cells within tree stems: implications for stem respiration modeling and scale-up. *Tree physiology* **20**, 1057–1062. (doi:10.1093/treephys/20.15.1057).

[9] Ceschia, r., Damesin, C., Lebaube, S., Pontailler, J.-Y. & Dufrne, r. 2002 Spatial and seasonal variations in stem respiration of beech trees (Fagus sylvatica). *Ann. For. Sci.* **59**, 801–812. (doi:10.1051/forest:2002078).

[10] Medina, N. G., Albertos, B., Lara, F., Mazimpaka, V., Garilleti, R., Draper, D. & Hortal, J. 2014 Species richness of epiphytic bryophytes: drivers across scales on the edge of the Mediterranean. *Ecography* **37**, 80–93. (doi:10.1111/j.1600-0587.2013.00095.x).

[11] Boch, S., Müller, J., Prati, D., Blaser, S. & Fischer, M. 2013 Up in the tree--the overlooked richness of bryophytes and lichens in tree crowns. *PloS one* **8**, e84913. (doi:10.1371/journal.pone.0084913).

[12] Rubio-Salcedo, M., Merinero, S. & Martínez, I. 2015 Tree species and microhabitat influence the population structure of the epiphytic lichen Lobaria pulmonaria. *Fungal Ecology* **18**, 1–9. (doi:10.1016/j.funeco.2015.08.002).

[13] Li, S., Liu, W.-Y., Li, D.-W., Song, L., Shi, X.-M. & Lu, H.-Z. 2015 Species richness and vertical stratification of epiphytic lichens in subtropical primary and secondary forests in southwest China. *Fungal Ecology* **17**, 30–40. (doi:10.1016/j.funeco.2015.02.005).

[14] Hedenås, H., Bolyukh, V. O. & Jonsson, B. G. 2003 Spatial distribution of epiphytes on Populus tremula in relation to dispersal mode. *Journal of Vegetation Science* **14**, 233–242. (doi:10.1111/j.1654-1103.2003.tb02148.x).

[15] Freystein, K., Salisch, M. & Reisser, W. 2008 Algal biofilms on tree bark to monitor airborne pollutants. *Biologia* **63**, 127. (doi:10.2478/s11756-008-0114-z).

[16] Steiner, M. & D. Schulze-Horn. 1955 Über die Verbreitung und Expositionsabhängigkeit der Rindenepiphyten im Stadtgebiet von Bonn. *Decheniana* **108.1**, 1–16.

[17] Illig, J., Norton, R. A., Scheu, S. & Maraun, M. 2010 Density and community structure of soil- and bark-dwelling microarthropods along an altitudinal gradient in a tropical montane rainforest. *Experimental & applied acarology* **52**, 49–62. (doi:10.1007/s10493-010-9348-x).

[18] Miller, K. M., Wagner, R. G. & Woods, S. A. 2007 Effect of gap harvesting on epiphytes and bark-dwelling arthropods in the Acadian forest of central Maine. *Can. J. For. Res.* **37**, 2175–2187. (doi:10.1139/X07-022).

[19] Chambers, J. Q., Higuchi, N., Schimel, J. P., Ferreira, L. V. & Melack, J. M. 2000 Decomposition and carbon cycling of dead trees in tropical forests of the central Amazon. *Oecologia* **122**, 380–388. (doi:10.1007/s004420050044).

[20] Malhi, Y., Aragao, Luiz Eduardo O. C., Metcalfe, D., Paiva, R., Quesada, C. A., Almeida, S., Anderson, L., Brando, P., Chambers, J. Q. & da Costa, Antonio C. L. *et al.* 2009 Comprehensive assessment of carbon productivity, allocation and storage in three Amazonian forests. Malhi, Yadvinder; Aragao, Luiz Eduardo O. C; Metcalfe, Dan; Paiva, Romilda; Quesada, Carlos A; Almeida, Samuel; Anderson, Liana; Brando, Paulo; Chambers, Jeffrey Q; da Costa, Antonio C. L; Hutyra, Lucy R; Oliveira, Paulo; Patino, Sandra; Pyle, Elizabeth H; Robertson, Amanda L; Teixeira, Liliane M. *Global Change Biology* **15**, 1255–1274. (doi:10.1111/j.1365-2486.2008.01780.x).

[21] MacFarlane, D. W. & Luo, A. 2009 Quantifying tree and forest bark structure with a bark-fissure index. *Can. J. For. Res.* **39**, 1859–1870. (doi:10.1139/X09-098).

[22] CARSTEN, L. D., JUOLA, F. A., MALE, T. D. & CHERRY, S. 2002 Host associations of lianas in a south-east Queensland rain forest. *J. Trop. Ecol.* **18**, 107–120. (doi:10.1017/S0266467402002067).

[23] OVINGTON, J. D. 1954 A COMPARISON OF RAINFALL IN DIFFERENT WOODLANDS. *Forestry* **27**, 41–53. (doi:10.1093/forestry/27.1.41).

[24] Pokorný, R. & Tomášková, I. 2008 Allometric relationships for surface area and dry mass of young Norway spruce aboveground organs. *J. For. Sci.* **53**, 548–554. (doi:10.17221/2166-JFS).

[25] Huang, P. & Pretzsch, H. 2010 Using terrestrial laser scanner for estimating leaf areas of individual trees in a conifer forest. *Trees* **24**, 609–619. (doi:10.1007/s00468-010-0431-z).

[26] Alonzo, M., McFadden, J. P., Nowak, D. J. & Roberts, D. A. 2016 Mapping urban forest structure and function using hyperspectral imagery and lidar data. *Urban Forestry & Urban Greening* **17**, 135–147. (doi:10.1016/j.ufug.2016.04.003).

[27] Alonzo, M., Bookhagen, B., McFadden, J. P., Sun, A. & Roberts, D. A. 2015 Mapping urban forest leaf area index with airborne lidar using penetration metrics and allometry. *Remote Sensing of Environment* **162**, 141–153. (doi:10.1016/j.rse.2015.02.025).

[28] Niklas, K. J., Cobb, E. D. & Spatz, H.-C. 2009 Predicting the allometry of leaf surface area and dry mass. *American journal of botany* **96**, 531–536. (doi:10.3732/ajb.0800250).

[29] Eyde, R. H. & Corner, E. J. H. 1976 Durian Theory. *Systematic Botany* **1**, 195. (doi:10.2307/2418777).

[30] White, P. S. 1983 Evidence that Temperate East North American Evergreen Woody Plants Follow Corner's Rules. *New Phytol* **95**, 139–145. (doi:10.1111/j.1469-8137.1983.tb03477.x).

[31] BROUAT, C., GIBERNAU, M., AMSELLEM, L. & McKEY, D. 1998 Corner's rules revisited: ontogenetic and interspecific patterns in leaf-stem allometry. *New Phytol* **139**, 459–470. (doi:10.1046/j.1469-8137.1998.00209.x).

[32] Zianis, D. 2005 *Biomass and stem volume equations for tree species in Europe.* Silva Fennica monographs, 1457-7356, 4, 2005. Helsinki, Finland: Finnish Society of Forest Science.

[33] Vallet, P., Dhôte, J.-F., Le Moguédec, G., Ravart, M. & Pignard, G. 2006 Development of total aboveground volume equations for seven important forest tree species in France. *Forest Ecology and Management* **229**, 98–110. (doi:10.1016/j.foreco.2006.03.013).

[34] Bentley, L. P., Stegen, J. C., van Savage, M., Smith, D. D., Allmen, E. I. von, Sperry, J. S., Reich, P. B. & Enquist, B. J. 2013 An empirical assessment of tree branching networks and implications for plant allometric scaling models. *Ecology letters* **16**, 1069–1078. (doi:10.1111/ele.12127).

[35] Danson, F. M., Disney, M. I., Gaulton, R., Schaaf, C. & Strahler, A. 2018 The terrestrial laser scanning revolution in forest ecology. *Interface focus* **8**, 20180001. (doi:10.1098/rsfs.2018.0001).

[36] Guo, H., Huang, Q., Li, X., Sun, Z. & Zhang, Y. 2014 Spatiotemporal analysis of urban environment based on the vegetation–impervious surface–soil model. *J. Appl. Remote Sens* **8**, 84597. (doi:10.1117/1.JRS.8.084597).

[37] Shao, G., Shao, G., Gallion, J., Saunders, M. R., Frankenberger, J. R. & Fei, S. 2018 Improving Lidar-based aboveground biomass estimation of temperate hardwood forests with varying site productivity. *Remote Sensing of Environment* **204**, 872–882. (doi:10.1016/j.rse.2017.09.011).

[38] Calders, K., Disney, M. I., Armston, J., Burt, A., Brede, B., Origo, N., Muir, J. & Nightingale, J. 2017 Evaluation of the Range Accuracy and the Radiometric Calibration of Multiple Terrestrial Laser Scanning Instruments for Data Interoperability. *IEEE Trans. Geosci. Remote Sensing* **55**, 2716–2724. (doi:10.1109/TGRS.2017.2652721).

[39] Rosell, J. R., Llorens, J., Sanz, R., Arnó, J., Ribes-Dasi, M., Masip, J., Escolà, A., Camp, F., Solanelles, F. & Gràcia, F. *et al.* 2009 Obtaining the three-dimensional structure of tree orchards from remote 2D terrestrial LIDAR scanning. *Agricultural and Forest Meteorology* **149**, 1505–1515. (doi:10.1016/j.agrformet.2009.04.008).

[40] Bauwens, S., Bartholomeus, H., Calders, K. & Lejeune, P. 2016 Forest Inventory with Terrestrial LiDAR: A Comparison of Static and Hand-Held Mobile Laser Scanning. *Forests* **7**, 127. (doi:10.3390/f7060127).

[41] Maas, H.-G., Bienert, A., Scheller, S. & Keane, E. 2008 Automatic forest inventory parameter determination from terrestrial laser scanner data. *International Journal of Remote Sensing* **29**, 1579–1593. (doi:10.1080/01431160701736406).

[42] Wilkes, P., Lau, A., Disney, M., Calders, K., Burt, A., Gonzalez de Tanago, J., Bartholomeus, H., Brede, B. & Herold, M. 2017 Data acquisition considerations for Terrestrial Laser Scanning of forest plots. *Remote Sensing of Environment* **196**, 140–153. (doi:10.1016/j.rse.2017.04.030).

[43] Åkerblom, M., Raumonen, P., Mäkipää, R. & Kaasalainen, M. 2017 Automatic tree species recognition with quantitative structure models. *Remote Sensing of Environment* **191**, 1–12. (doi:10.1016/j.rse.2016.12.002).

[44] Raumonen, P., Casella, E., Calders, K., Murphy, S., Åkerbloma, M. & Kaasalainen, M. 2015 Massive-scale tree modelling from TLS data. *ISPRS Ann. Photogramm. Remote Sens. Spatial Inf. Sci.* **II-3/W4**, 189–196. (doi:10.5194/isprsannals-II-3-W4-189-2015).

[45] Raumonen, P., Kaasalainen, M., Åkerblom, M., Kaasalainen, S., Kaartinen, H., Vastaranta, M., Holopainen, M., Disney, M. & Lewis, P. 2013 Fast Automatic Precision Tree Models from Terrestrial Laser Scanner Data. *Remote Sensing* **5**, 491–520. (doi:10.3390/rs5020491).

[46] Dassot, M., Constant, T. & Fournier, M. 2011 The use of terrestrial LiDAR technology in forest science: application fields, benefits and challenges. *Ann. For. Sci.* **68**, 959–974. (doi:10.1007/s13595-011-0102-2).

[47] Good, N. M., Paterson, M., Brack, C. & Mengersen, K. 2001 Estimating tree component biomass using variable probability sampling methods. *JABES* **6**, 258–267. (doi:10.1198/108571101750524599).

[48] Gregoire, T. G., Valentine, H. T. & Furnival, G. M. 1995 Sampling Methods to Estimate Foliage and Other Characteristics of Individual Trees. *Ecology* **76**, 1181–1194. (doi:10.2307/1940925).

[49] Unterseher, M., Otto, P. & Morawetz, W. 2005 Species richness and substrate specificity of lignicolous fungi in the canopy of a temperate, mixed deciduous forest. *Mycol Progress* **4**, 117–132. (doi:10.1007/s11557-006-0115-7).

[50] Deutscher Wetter Dienst *Niederschlag: vieljährige Mittelwerte 1981 - 2010 Leipzig*. See https://www.dwd.de/DE/leistungen/klimadatendeutschland/mittelwerte/nieder_8110_akt_html.html?view=nasPublication&nn=17626.

[51] Goddert von Oheimb & Dr. Matthias Kunz. 2018 – 2018 *Projektbericht: AZ 31967-2017, Dreidimensionale Erfassung der Waldbestandsstruktur um den Leipziger Auwaldkran mittels terrestrischem Laserscanning*.

[52] Reiher, A. 2006 *Diversität, vertikale Verteilung und saisonale Aspekte von blattbewohnenden endophytischen Pilzen im Kronenraum des Leipziger-Auwaldkran Untersuchungsgebietes. Universität Leipzig, Diplomarbeit*. Dimplom.

[53] van der Zande, D., Hoet, W., Jonckheere, I., van Aardt, J. & Coppin, P. 2006 Influence of measurement set-up of ground-based LiDAR for derivation of tree structure. *Agricultural and Forest Meteorology* **141**, 147–160. (doi:10.1016/j.agrformet.2006.09.007).

[54] RIEGL - Laser Measurement Systems GmbH. 2018 *RiSCAN PRO*. *for RIEGL 3D Laser Scanners:* RIEGL.

[55] Daniel Girardeau-Montaut. 2019 *CloudCompare version 2.6.3.1*. *Détection de changement sur des données géométriques tridimensionnelles*.

[56] Computree Core Team. 2017 *A processing platform for 3D points clouds in forestry*. *Plugin Base for Computree:* Computree Group.

[57] Jules Morel Method developed during the Ph.D of Jules Morel supported by IFPand LSIS .Plugin extended with the support of AMAP and the Computree Core Team. Plugin. See http://www.ifpindia.org/; http://amap.cirad.fr.

[58] Hackenberg, J., Spiecker, H., Calders, K., Disney, M. & Raumonen, P. 2015 SimpleTree —An Efficient Open Source Tool to Build Tree Models from TLS Clouds. *Forests* **6**, 4245–4294. (doi:10.3390/f6114245).

[59] Hackenberg, J., Wassenberg, M., Spiecker, H. & Sun, D. 2015 Non Destructive Method for Biomass Prediction Combining TLS Derived Tree Volume and Wood Density. *Forests* **6**, 1274–1300. (doi:10.3390/f6041274).

[60] Rusu, R. B., Marton, Z. C., Blodow, N., Dolha, M. & Beetz, M. 2008 Towards 3D Point cloud based object maps for household environments. *Robotics and Autonomous Systems* **56**, 927–941. (doi:10.1016/j.robot.2008.08.005).

[61] CloudCompare. 2019 *Statistical Outlier Removal*. See cloudcompare.org/doc/wiki/index.php?title=SOR_filter.

[62] Raumonen, P. 2017 *TreeQSM - Quantitative Structure Models of Single Trees from Laser Scanner Data*. *Instructions for MATLAB-software TreeQSM, version 2.30.*

[63] R Core Team 2019. op. 2010 *R*. *A language and environment for statistical computing : reference index.* [Vienna]: R Foundation for Statistical Computing.

[64] Madgwick, H. A. I. & Satoo, T. 1975 On Estimating the Aboveground Weights of Tree Stands. *Ecology* **56**, 1446–1450. (doi:10.2307/1934713).

[65] Akaike, H. 2011 Akaike's Information Criterion. In *International Encyclopedia of Statistical Science* (ed. M. Lovric), p. 25. Berlin, Heidelberg: Springer Berlin Heidelberg.

[66] Yang, D., Niklas, K. J., Xiang, S. & Sun, S. 2010 Size-dependent leaf area ratio in plant twigs: implication for leaf size optimization. *Annals of botany* **105**, 71–77. (doi:10.1093/aob/mcp262).

[67] Westoby, M., Falster, D. S., Moles, A. T., Vesk, P. A. & Wright, I. J. 2002 Plant Ecological Strategies: Some Leading Dimensions of Variation Between Species. *Annu. Rev. Ecol. Syst.* **33**, 125–159. (doi:10.1146/ANNUREV.ECOLSYS.33.010802.150452).

[68] Burt, A., Disney, M. & Calders, K. 2018 Extracting individual trees from lidar point clouds using treeseg. *Methods Ecol Evol*. (doi:10.1111/2041-210X.13121).

[69] Paynter, I., Genest, D., Peri, F. & Schaaf, C. 2018 Bounding uncertainty in volumetric geometric models for terrestrial lidar observations of ecosystems. *Interface focus* **8**, 20170043. (doi:10.1098/rsfs.2017.0043).

Fig. 17. Sub-sampled point cloud of *Q. robur* ID: 129. The tree with the largest measured diameter at breast height of 1.35 m, with a hight of 32.27 m a volume of 34.66 m^3, a woody surface area of 913.73 m^2, with a maximum branch order of 12 and 14 925 branches. Next to it, a scan of Dr. Mathias Kunz and Ronny Richter.